Substructure of the Outer Dynein Arm

URSULA W. GOODENOUGH and JOHN E. HEUSER
Departments of Biology and Physiology/Biophysics, Washington University, St. Louis, Missouri 63130

ABSTRACT The substructure of the outer dynein arm has been analyzed in quick-frozen deep-etch replicas of *Tetrahymena* and *Chlamydomonas* axonemes. Each arm is found to be composed of five morphologically discrete components: an elliptical head; two spherical feet; a slender stalk; and an interdynein linker. The feet make contact with the A microtubule of each doublet; the stalk contacts the B microtubule; the head lies between the feet and stalk; and the linker associates each arm with its neighbor. The spatial relationships between these five components are found to be distinctly different in rigor (ATP-depleted) *versus* relaxed (ATP- or vanadate plus ATP-treated) axonemes, and the stalk appears to alter its affinity for the B microtubule in the relaxed state. Images of living cilia attached to *Tetrahymena* cells show that the relaxed configuration is adopted in vivo. We relate our observations to morphological and experimental studies reported by others and propose several models that suggest how this newly described dynein morphology may relate to dynein function.

Doublet microtubules of eukaryotic cilia and flagella are bridged by outer dynein arms that are presumed to play a key role in the mechanochemical generation of ciliary motility (see references 6, 16, and 54 for recent reviews). Considerable progress has been made in analyzing the polypeptide components and the ATPase activities associated with the outer arms (11, 49, 64), and both biochemical and morphological studies indicate that each arm must be composed of several subunits (19, 49, 64, 70). To date, however, the number, size, and spatial relationships of these postulated subunits remain unknown, largely because the arms are poorly resolved when viewed by traditional thin section or negative-stain electron microscopy. Two factors are likely to contribute to this poor resolution: the arms may well be sensitive to such manipulations as fixation, dehydration, and air drying; moreover, because they repeat along each doublet with a 24-nm period and span a 21-nm inter-doublet gap, there is likely to be considerable image overlap in both thin-sectioned and negatively stained preparations.

The quick-freeze, deep-etch technique (24) is well suited to the study of structures such as dynein arms, since material can be examined without chemical fixation, dehydration, or staining, and the resultant three-dimensional platinum replicas are free of image superimposition. When care is taken to examine only material that is optimally frozen, meaningful images of high resolution can be obtained.

Using this technique, we have analyzed the substructure of outer dynein arms in axonemes (demembranated cilia) of *Tetrahymena* and *Chlamydomonas*. We show that each outer arm consists of five discrete structural components, and we document the distinct configurations adopted by these subunits under two extreme conditions: *rigor*, in which the axonemes are fully depleted of ATP, and *relaxation*, in which the axonemes are presented with ATP plus sodium vanadate, a dynein ATPase inhibitor (17, 35). We demonstrate that the relaxed configuration is also adopted by outer arms in the presence of ATP alone, and we show that a comparable structural configuration is found in vivo. We conclude that ATP converts the dynein arm from a locked conformation to a more open conformation, and we consider how this conversion might function during the ciliary beat.

MATERIALS AND METHODS

Isolation of Chlamydomonas Flagella

Wild-type *Chlamydomonas reinhardi* gametes (10^{10} of each mating type) were harvested from agar plates (42), washed in nitrogen-free high-salt minimal medium (NFHSM) (61), and allowed to mate for 30 min to form motile quadriflagellate cells. During the mating reaction, released cell-wall fibers were removed by two washes in 1 l of NFHSM, followed by a wash in 250 ml of HMDS buffer (10 mM HEPES, pH 7.4; 5 mM $MgSO_4$; 1 mM DTT; 4% sucrose) (73).

Deflagellation and flagellar isolation were generally according to the procedure of Witman et al. (73). Washed cells were suspended in 25 ml of HMDS, pipetted into a tube containing 5 ml of 25 mM dibucaine HCl (CIBA-GEIGY, CIBA Pharmaceutical Co., Summit, NJ), and sucked up and down gently until deflagellation was quantitative (usually <1 min). The suspension was then mixed with 50 ml of cold HMDS containing 0.25 mM EGTA. Cells were pelleted by a brief spin at 1,200 *g*, followed by a 7 min spin at 1,200 *g*; flagella were then pelleted by centrifugation at 12,000 *g* for 15 min. Flagella were demembranated by suspending in 10 ml of cold 1% NP-40 (Nonidet P-40, Particle Data Labs Ltd.) buffered in HMDEK (30 mM HEPES, pH 7.4; 5 mM $MgSO_4$; 1 mM DTT; 2 mM EGTA; 25 mM KCl) for 5–15 min. The axonemes were pelleted at 10,000 *g* for 5 min and washed once in HMDEK.

THE JOURNAL OF CELL BIOLOGY · VOLUME 95 DECEMBER 1982 798–815

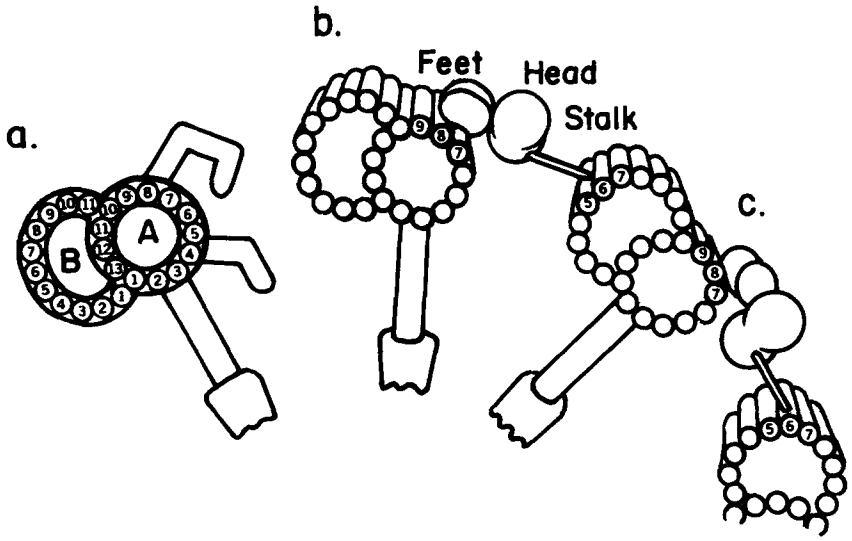

FIGURE 1 Cross-sectional diagram of a ciliary axoneme, adapted from Warner (67), with the numbering of the A and B protofilaments according to Tilney et al. (66). (*a*) Outer arm as it appears in traditional thin-section images of living cilia. The inter-doublet gap is wider than in the original drawing (67) to conform to the gap dimensions found in deep-etch replicas. (*b*) Outer arm in rigor as it appears in deep-etch replicas. (*c*) Outer arm in the relaxed conformation as it appears in deep-etch replicas.

Isolation of Tetrahymena Cilia

Tetrahymena thermophila, strain B-1868, was cultured in axenic medium as described (21). 500 ml of mid-log phase cells were harvested by brief gentle centrifugation (650 *g*) and were deciliated by one of two protocols. Protocol A, utilized for most samples, is essentially that of Witman et al. (73) as described above for *Chlamydomonas*. Protocol B, utilized for several samples, is essentially that of Mitchell and Warner (44): cells were harvested and suspended in 50 ml of fresh culture medium (2% proteose peptone, 0.2% glucose, and 0.1% yeast extract); to this was added 10 ml of 10 mM dibucaine. After deciliation (which requires at least 2 min), the suspension was diluted with an equal volume of fresh culture medium; cells were pelleted by repeated short, slow centrifugations (1,000 *g*); cilia were then pelleted by a 12,000 *g* spin for 15 min. The pellet was suspended in 5 ml of HMEK buffer (10 mM HEPES, pH 7.4; 5 mM $MgSO_4$; 0.5 mM Na_2EDTA; 100 mM KCl), to which was added an equal volume of 0.4% Triton X-100 (Sigma Chemical Co., St. Louis, MO) in HMEK for 15 min; the demembranated axonemes were pelleted at 12,000 *g* for 5 min and resuspended in 5 mM $MgSO_4$, 10 mM HEPES, pH 7.4. ATP was added in this buffer.

The rigor axonemes produced by each protocol, although indistinguishable in fine structure, respond very differently to ATP: protocol-B axonemes undergo "spontaneous" sliding disintegration when exposed to ATP (69, 71), whereas protocol-A axonemes reactivate (undergo ciliary bending) in the presence of ATP, and require exogeneous protease to induce sliding disintegration. We suspect that some feature of protocol B stimulates proteolysis of the axonemes.

Reagents and Fixation

ATP (vanadate-free) (Sigma Chemical Co.) was prepared as a 1–25 mM MgATP stock solution in HMDEK titrated to pH 7.4. Sodium vanadate (Fisher Scientific Co., Pittsburgh, PA) was prepared as a 10 mM stock solution in distilled water. Glutaraldehyde (Ladd Research Industries, Inc., Burlington, VT) was prepared as a 4% stock solution in the buffer (plus any additives) containing the samples; final fixative concentrations were 1–2%. Fixation was for 30 min at 4°, followed by a wash in HMDEK.

Sample Preparation for Electron Microscopy

Immediately before freezing, each sample was pelleted and resuspended in a small volume of supernatant to produce a concentrated slurry of axonemes. ~10 μl (~40 mg axonemal protein) was then pipetted onto the surface of a thin slab of aldehyde-fixed lung (24). Freezing was accomplished with the helium-cooled, copper-block device developed in this laboratory (28).

Freeze-fracturing and etching were modified in two respects. To ensure that exposed areas would be optimally frozen, fracturing was reduced to an absolute minimum: the plane of cleavage entered the sample only a few microns beneath its surface, and large regions of the surface were not cleaved at all. To limit the depth of exposure around the organelles to ~0.1 μm, etching was minimized: the specimen temperature was lowered to −105°C, and etching time was reduced to about 2 min.

Samples were rotary-replicated with platinum and carbon as described previously (25, 26). Evaporation of carbon was reduced to 3–5 s to minimize the thickness of the carbon backing film and thereby prevent "ghost images" from appearing around the delicate components in these replicas. Replica cleaning was improved by immersing the samples in full-strength chromate cleaning solution (Fisher Scientific Co.) rather than in household bleach.

Orientation of Replicas

To determine whether a negative was being viewed right-side-up, we initially utilized the orientation of the three-start helix of the microtubules, which should appear right-handed when viewed in a correctly oriented microtubule interior (3). The base-to-tip orientation of an axoneme could also be identified directly if either its singlet-microtubule tip or its differentiated base were exposed. We soon recognized that when an axoneme is viewed right-side-up and with its base pointing downwards, the B microtubule of each doublet lies to the left of the A tubule bearing the bulky end of the outer dynein arm, and the arms and/or their slender stalks always tilt towards the base. Therefore, the B/A position and the basal tilt of the arms became the criteria by which we oriented most of our negatives.

Sample Size and Consideration of Artifacts

For this study, 350 samples were replicated and 65 replicas were photographed extensively. Individual axonemes were chosen for photography solely on the basis of their optimal freezing, with little initial information on their experimental history. At least 25–50 high magnification (≥70,000×) stereo views were obtained of each sample, and micrographs of >5,000 axonemes were analyzed during the course of this study.

In spite of the unusually low temperatures used in our freezing process, major areas in all of our replicas displayed inadequate freezing, usually recognizable by a crystalline texture in the ice surrounding the axonemes. Two artifacts were found to accompany inadequate freezing: the substructure of the outer dynein arms cannot be resolved, and the axonemes become compressed in diameter such that the outer-arm heads come to make contact with the B tubules and the stalks are obscured. Axonemes frozen at the air/water interface are often similarly compressed (see Fig. 28), possibly because evaporation has increased the concentrations of ions in their immediate vicinity (see, in this regard, references 15, 55, 68, and 76).

Three additional sources of artifact in our preparative methods have recently been suggested: (*a*) detergent might remove relevant structures (56); (*b*) salts might precipitate to form adventitious structures (43); and (*c*) structures might be flattened during the freezing process (48). None of these appears to be a problem here. We will document in *Results* that: (*a*) outer-arm substructure in the living state is identical to its structure after detergent extraction; (*b*) axonemes fixed in glutaraldehyde and then washed and frozen in distilled water look identical to those frozen in a salt solution; and (*c*) three-dimensional images show that frozen axonemes have the expected cylindrical structure.

RESULTS

Model of Outer Arm Substructure in Rigor

Fig. 1 diagrams three of the nine microtubule doublets of a ciliary axoneme. Fig. 1 *a* shows an outer dynein arm as it would

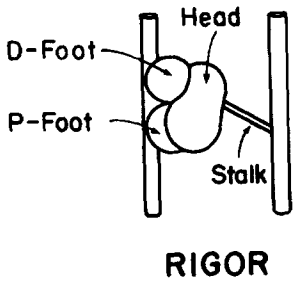

FIGURE 2 Diagram of the outer arm in rigor as it appears in frontal view in deep-etch replicas. The A microtubule of one doublet is on the left; the B microtubule of its neighboring doublet is on the right. The linker has been omitted for simplicity; its rigor disposition is diagrammed in Fig. 23.

appear in traditional thin-section images (2). The "A end" (65) of the arm is depicted as a straight component that extends diagonally outward from the A microtubule, and the "B end" is represented as a larger hook-shaped component that extends towards the B microtubule of the adjacent doublet. The B end does not ordinarily appear to make contact with the B microtubule, leaving an interdoublet "gap."

Figs. 1*b* and 2 diagram cross-sectional and frontal views of rigor (ATP-depleted) outer arms based on our interpretation of quick-frozen deep-etched replicas. We present the diagrams before the replicas so that the electron micrographs can be viewed with some landmarks in mind. Each dynein arm is shown to be composed of five physically distinct components. To facilitate their initial description, we have given them morphological names; these, we trust, will be replaced by more appropriate, functional names once the contribution of each component to ciliary motility is elucidated.

HEAD AND STALK: The head and stalk form a complex having the general shape of a croquet mallet viewed from the side. The stalk extends from the side of the "mallet head' to the B microtubule, thus spanning the inter-doublet gap. The head appears to correspond to the traditional "B end" or hook of the outer dynein arm.

FEET: The feet lie side-by-side in pairs on the A microtubule and appear to account for the traditional "A end" of the outer arm. The more proximal foot in each pair (i.e., the one closer to the base of the cilium) is denoted the *P-foot* and the more distal the *D-foot*. The head ordinarily rests against both feet in the rigor configuration.

LINKER: This component is inconspicuous in rigor axonemes and is therefore not included in Figs. 1 and 2, but becomes prominent after exposure to ATP. In rigor, it usually extends from the distal aspect of one head towards the P-foot of the next dynein arm.

Overall Distribution of Dynein Arms in Rigor

Fig. 3 shows in 3-D two rigor axonemes from *Tetrahymena* that were initially fractured obliquely; subsequent etching has exposed portions of their axonemal shafts. The cross-fractured portions of each axoneme show two central microtubules surrounded by radial spokes that extend from the central sheath to each of the nine peripheral doublets. The A microtubule of each doublet is known to make contact with a radial spoke (c.f. Fig. 1); by this criterion, the A microtubules lie to the right of the B microtubules in these axonemes, and both are oriented as if viewed from base to tip (13). Outer dynein arms stud the peripheral doublets with a 24-nm periodicity. The bulky base of each arm is seen to associate with the outer surface of an A microtubule (Fig. 3, arrow), and a slender stalk extends from each arm to the contiguous B microtubule.

Figs. 4–10 show *Tetrahymena* and *Chlamydomonas* axonemes that were frozen while in the rigor state and happened to be lying parallel to, but immediately beneath, the plane of freeze fracture. They were subsequently exposed by subliming away the surrounding ice, providing lengthwise views of the microtubule doublets from an aerial perspective. These and subsequent "aerial views" are mounted so that the proximal end of each axoneme points towards the bottom or the left of the figure. Thus within each doublet, the B microtubule lies to the left or above the A microtubule. The axonemes shown in Figs. 4 and 5 were fixed in 1% glutaraldehyde; Figs. 6–10 show axonemes that were frozen without prefixation. There were no substantial differences between fixed and unfixed samples. The following sections describe the substructure of the five outer-arm components as they appear in these deep-etch replicas.

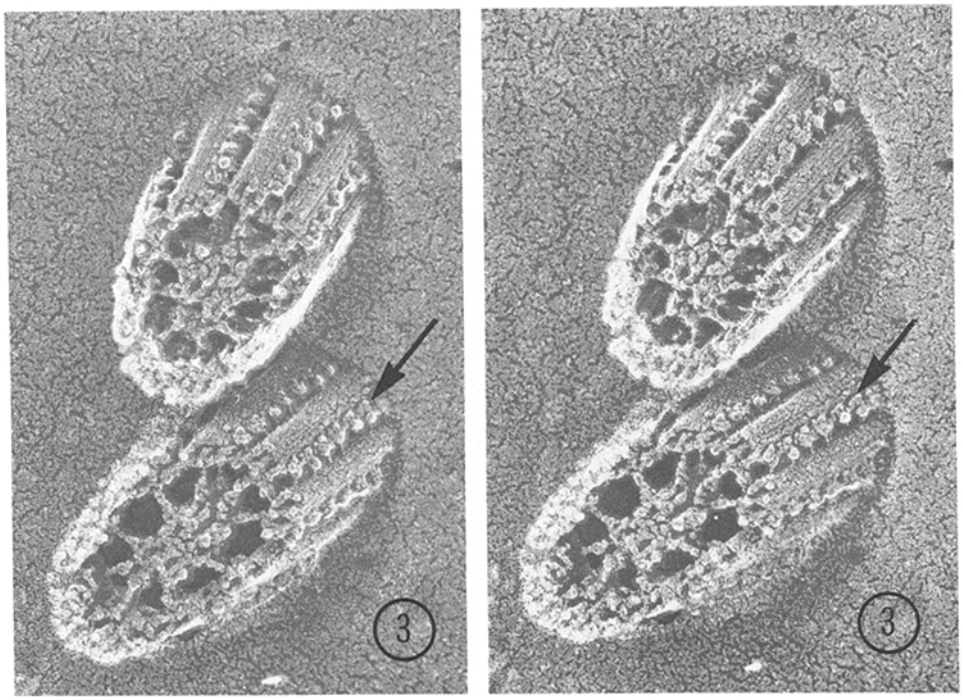

FIGURE 3 Rigor *Tetrahymena* axonemes, glutaraldehyde-fixed and fractured obliquely to their cross-sectional axes, stereo pair. The axonemes were washed in water to remove surrounding salts, producing the smooth background. The arrow indicates a particularly distinct row of outer dynein arms. This and subsequent stereo pairs should be viewed with the aid of a pocket stereoscope (Taylor-Merchant Corp., New York, NY) or by the more direct ocular-divergence method explained by Wolosewick and Porter (74). × 115,000.

The Stalk in Rigor

The stalk is about 11 nm in length and about 2 nm in width in delicately shadowed replicas. In rigor axonemes, the stalk attaches to the head of the dynein arm at an eccentric, slightly distal position and inclines basally to attach to the B microtubule (Figures 4–6, 8). The angle of inclination, while somewhat variable, averages 14° from the perpendicular and serves as a useful guide for locating the proximal end of the axoneme.

Close scrutiny of the middle rows of Figs. 5, 6, and 8 show that some stalks contact the B microtubule at a deep position whereas others attach at a higher level. Using the numbering system given in Fig. 1, stalks within individual rows have been observed to contact protofilaments #5, 6, or 7 of the B tubule. It is not possible to resolve whether the stalk attaches directly to a protofilament or to a site between two protofilaments; either possibility is consonant with its molecular dimensions.

Rigor axonemes obtained from *Chlamydomonas* retain the curved waveforms that characterize their native beat. The 21-nm gap that separates doublets in straight regions of the axoneme continues to separate doublets in these curved regions, and the stalks continue to bridge the distance between the outer arms and the B tubules. Therefore, if the curved shapes of rigor-wave axonemes are indeed maintained by the outer arms,

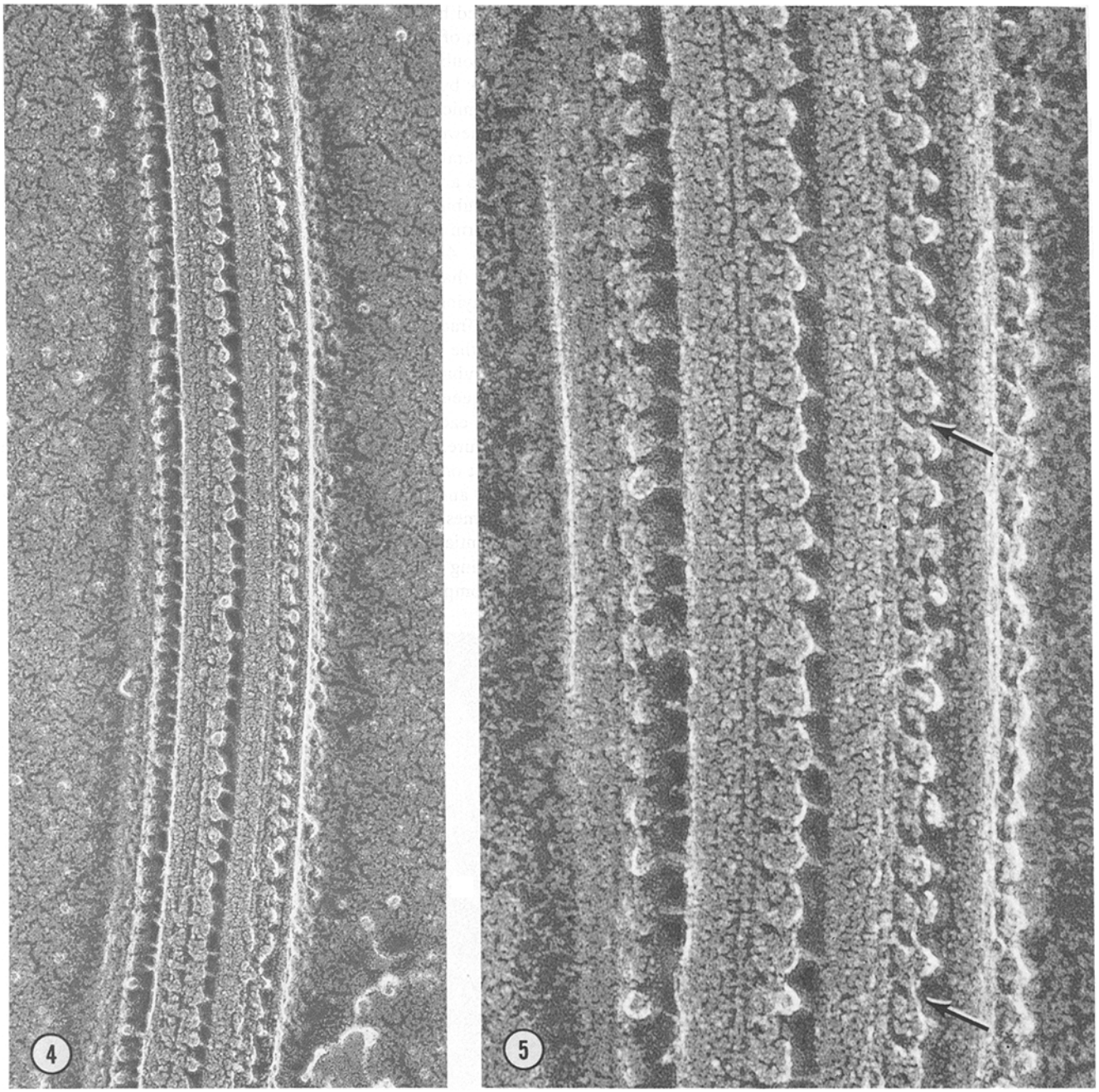

FIGURES 4 and 5 Fig. 4. Rigor *Tetrahymena* axoneme, glutaraldehyde-fixed, showing dynein arms seen by the four different vantage points provided by deep etching. × 145,000. Fig. 5. Rigor *Tetrahymena* axoneme, glutaraldehyde-fixed, giving a higher-magnification view of the four outer-arm rows. Lower arrow denotes a typical example of the linkers found between each dynein's head and its neighbor's P-foot. Upper arrow denotes a linker whose origin and insertion are not visible, but which appears to extend towards its neighbor's head. × 350,000.

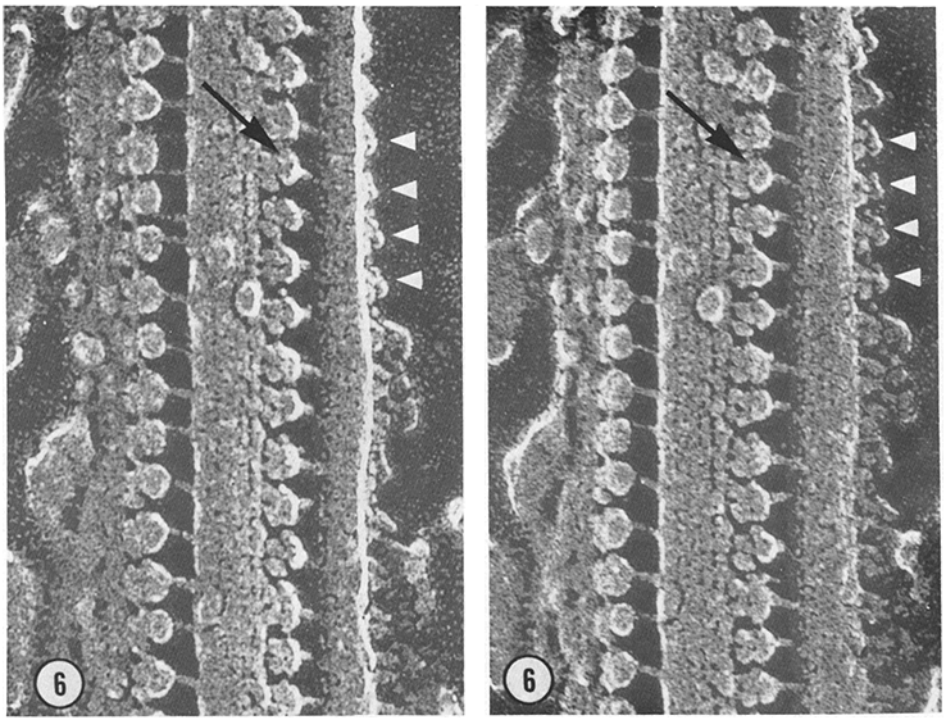

FIGURE 6 Rigor *Chlamydomonas* axoneme, unfixed, stereo pair. The head-feet-stalk substructure of the outer arm is seen to advantage in the right-hand row. The arrow denotes one instance in which a head appears more circular and associates with the D-foot; several other examples of this are present in the same row. The arrowheads on the far right indicate dynein heads in "horizon view" whose dimeric substructure is evident. × 272,000.

as suggested by the experiments of Gibbons and Gibbons (10), then these configurations would appear to be mediated, at least in part, by the delicate stalks.

The Feet in Rigor

Outer-arm feet occupy a highly invariant position on the A microtubule. The central doublets in Figs. 4 and 5 display to advantage a longitudinal "seam" that represents the junction between the walls of the B and A microtubules (c.f. Fig. 1). The protofilament to the right of this seam (A protofilament #9) appears wider than the others, perhaps reflecting a unique biochemical composition (36, 38), and the feet rest on the protofilament immediately to the right of this wide protofilament (A protofilament #8) (Figs. 4–10).

Each foot measures ~9 nm in diameter; therefore, each pair of feet is ~18 nm in length and is separated from its neighbor by a space of ~6 nm. Both feet appear roughly spherical from all angles of viewing. In *Tetrahymena*, the P-foot tends to be shifted back slightly towards protofilament A7, causing the D-foot to appear more prominent (Fig. 9), a tendency not found in *Chlamydomonas* (Fig. 10).

The Head in Rigor

In direct frontal views such as Figs. 6–8, most rigor heads are elliptical in shape, measuring ~17 nm along their proximal-distal axis and ~13 nm along their shorter circumferential axis. Their longer dimension is similar to a pair of feet (18 nm in the proximal-distal direction); hence the edges of the elliptical rigor heads parallel the edges of their feet.

Roughly 10% of rigor heads appear instead more circular, measuring ~13 nm along both axes. These associate exclusively with the D-foot; an example is denoted by the arrow in Fig. 6. Such images appear to arise when the head loses its association with the P-foot and pivots on the D-foot so that a "pounding surface" of the mallet comes to face the viewer. The relative infrequency of these images suggests that the pivoting may be induced during specimen preparation, but it serves to provide a view of the end of the head, and it suggests that the rigor

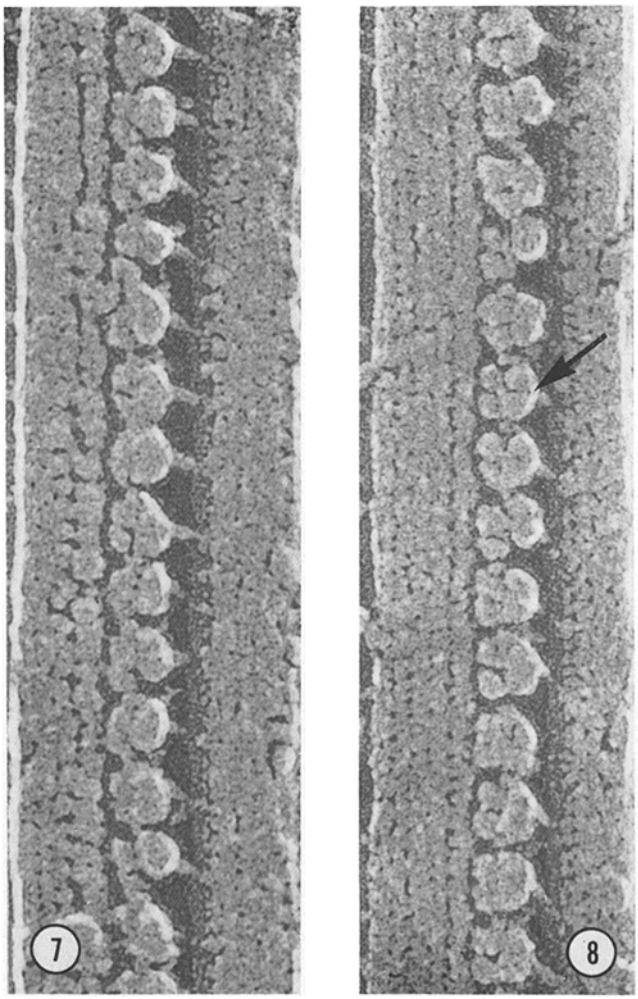

FIGURES 7 and 8 Fig. 7. Rigor *Chlamydomonas* axoneme, untixed, showing to advantage the varying levels on the B microtubule to which the stalks attach. × 380,000. Fig. 8. Rigor *Chlamydomonas* axoneme, unfixed. Arrow denotes a conspicuous medial cleft within one head, suggesting a dimeric substructure. × 440,000.

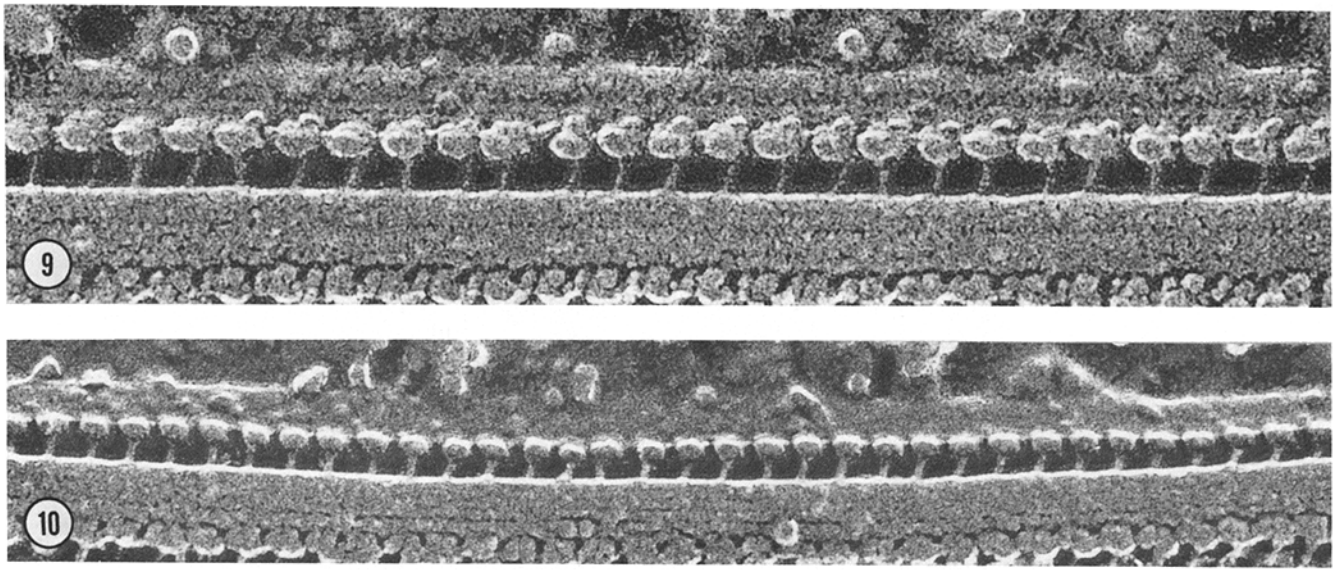

FIGURES 9 and 10 Fig. 9. Rigor *Tetrahymena* axoneme, unfixed, showing arms in the same orientation as Fig. 10. Note that the D-foot is more prominent than the P-foot. × 235,000. Fig. 10. Rigor *Chlamydomonas* axoneme, unfixed, showing the disposition of the stalk insertion sites at the backs of the heads. × 235,000.

head has a stronger affinity for the D-foot than the P-foot.

In the more typical elliptical view, the long axis of the head occasionally exhibits a dimeric substructure. This bifidity is most conspicuous in the head denoted by an arrow in Fig. 8; with this image in mind, a similar differentiation can be detected in other heads along with the same row. The dimeric configuration is also evident in the right-hand row of Fig. 6, where the heads of several dynein arms (arrowheads) are seen from the side.

As illustrated in the model portrayed in Fig. 2, the rigor head appears to be slewed with respect to the feet such that its distal aspect points toward the center of the axoneme. From the perspective of the right-hand row of Fig. 6, this slew is seen as a slight prominence of the proximal half of each head relative to its distal half. A direct view of the disposition of the head is provided by longitudinal fractures that pass through the centers of axonemes, exposing inter-doublet gaps from which the viewer can look down on the heads from the perspective of their stalks. From this vantage point, the head is sloped at an angle of ~45° from the perpendicular, with its distal aspect pointing toward the axoneme interior (see also reference 72).

The stalk attachment site of the dynein head is seen to advantage in Figs. 9 and 10 and in the left-hand row of Fig. 6. The stalks attach at uniformly eccentric positions that appear to be deep (i.e., toward the center of the axoneme) relative to their attachment sites on the B microtubules.

The Linker in Rigor

Close inspection of the elliptical rigor heads in aerial view reveals an asymmetry: the distal aspect of each ellipse has an extended, tapered appearance not found on the proximal side (Figs. 6–8). These distal extensions, which we denote as linkers, vary considerably in shape and prominence, appearing as flares, punctate elements, or strands. This variability is apparently caused in part by shifts in head orientation that expose the linkers to different extents, but it may also reflect real differences in linker deposition along a dynein row.

Optimal resolution of the rigor linker is provided by the right-center row of Fig. 5. The arm denoted by the lower arrow demonstrates to advantage that the proximal end of each linker attaches to the outermost distal aspect of each head. In ~10% of the cases, the linker appears to extend straight toward the head of the next dynein arm (Fig. 5, upper arrow), but in most cases (Fig. 5, lower arrow) it angles toward the P-foot of the adjacent dynein arm and usually appears to contact the P-foot directly.

Motility Induced by ATP and Inhibited by Vanadate

We have analyzed the motility induced by exposure of *Tetrahymena* and *Chlamydomonas* axonemes to ATP. Under our preparative conditions, the doublets remain associated with one another during the in vitro beat, i.e., they do not undergo sliding disintegration (62, 69). We have also analyzed the effect of sodium vanadate on this in vitro beat. Preincubation of *Chlamydomonas* axonemes with 10–200 μM vanadate alone has no effect on the incidence of rigor waveforms in the light microscope, and the outer arms display a normal rigor structure in platinum replicas. Addition of ATP to these vanadate-treated axonemes cause the rigor waveforms to "relax" (45, 51) such that, by light microscopy, each axoneme appears slack, drooping slightly at either end like an archer's bow. Although we have no information on the response to ATP during the few seconds taken to prepare a slide for light microscopy, vanadate plus ATP-treated axonemes exhibit no motility from the moment of viewing.

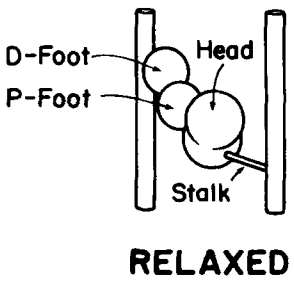

FIGURE 11 Diagram of the outer arm in the relaxed configuration as it appears in frontal view in deep-etch replicas. The A microtubule of one doublet is on the left; the B microtubule of its neighboring doublet is on the right. The linker has been omitted for simplicity; its relaxed disposition is diagrammed in Fig. 23.

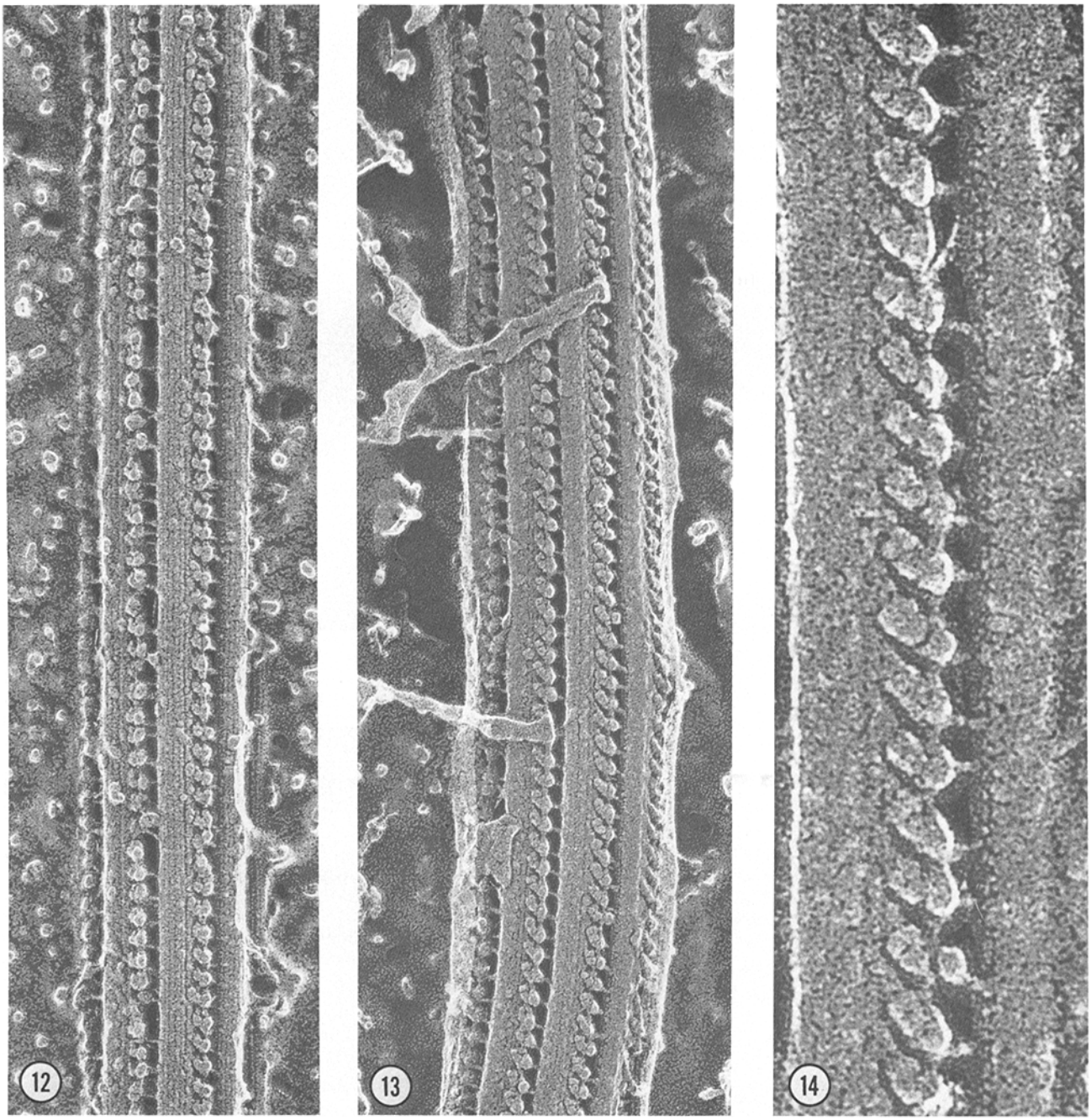

FIGURE 12–14 Fig. 12. Relaxed *Chlamydomonas* axoneme, unfixed, incubated in 0.2 mM vanadate followed by 1 mM ATP. Survey view of arm disposition. × 145,000. Fig. 13. Relaxed *Tetrahymena* axoneme, unfixed, incubated in 0.1 mM vanadate and then 0.5 mM ATP. Survey view of arm disposition. × 145,000. Fig. 14. Relaxed *Tetrahymena* axoneme, unfixed, incubated in 0.5 mM ATP, showing arm disposition at higher magnification. Feet are tilted proximally, and head associates with the P-foot. × 465,000.

Outer-arm Substructure in ATP and in Vanadate Plus ATP

The outer dynein arms undergo a dramatic change in conformation in the presence of ATP. This same change occurs if the axonemes are first pretreated with vanadate; therefore, it is a response to ATP and not a reflection of ongoing motility *per se*. Fig. 2*c* diagrams such an arm as it would appear in cross-section, and Fig. 11 diagrams our interpretation of its structure in frontal view. We refer to this configuration as "relaxed" to emphasize its most conspicuous morphological difference from rigor, namely, that the components are less compactly associated with one another.

Comparison of Figs. 11 and 2 reveals five features that distinguish the relaxed arm from the rigor arm. (*a*) The relaxed head loses its association with the D-foot and maintains contact exclusively with the P-foot. (*b*) The head rotates so that its distal "pounding surface" swings down toward the axonemal interior. (*c*) The stalk appears to insert into the head at a more proximal position, apparently as a consequence of the head rotation. (*d*) Each linker element shifts its position so as to make direct contact with the basal aspect of the adjacent dynein head. (*e*) The P-foot is no longer constrained to contact the A tubule, particularly in *Tetrahymena*, and can extend quite far out into the inter-doublet space, carrying its associated head along with it, so that the entire arm displays a steep basal tilt.

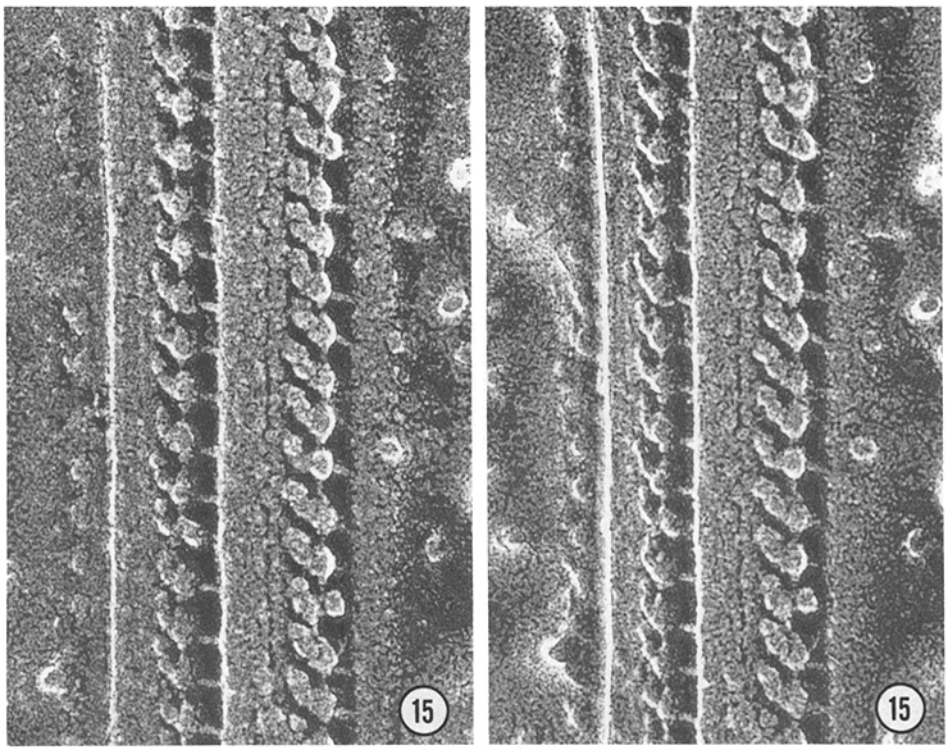

FIGURE 15 Relaxed *Tetrahymena* axoneme, unfixed, incubated in 0.1 mM vanadate and then 0.5 mM ATP. Stereo pair. P-foot detachment from the A microtubule is shown to advantage, as are the head-to-head linkers in both rows. Some stalks tilt more basally than others. × 270,000.

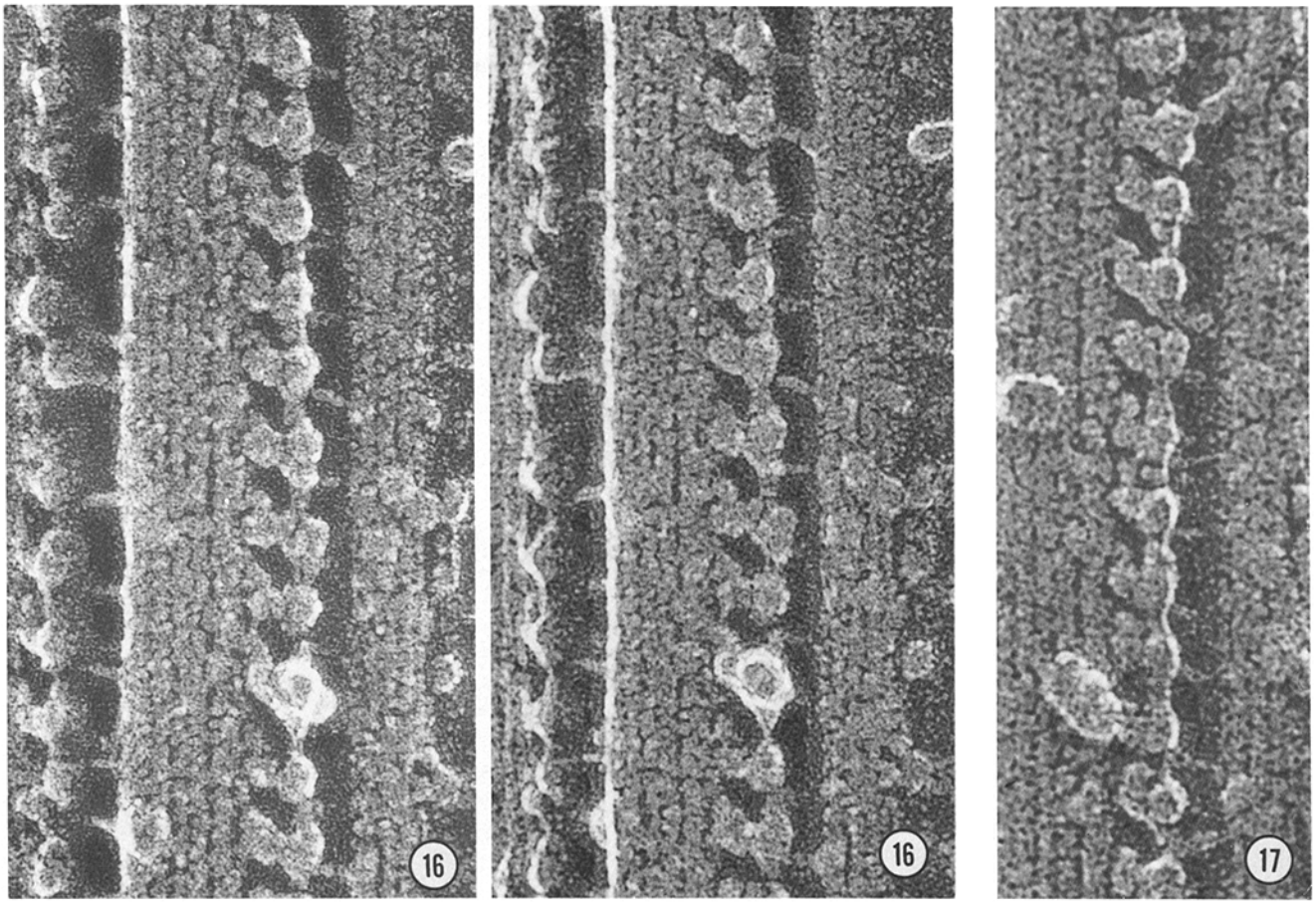

FIGURES 16 and 17 Fig. 16. Relaxed *Chlamydomonas* axoneme, unfixed, incubated in 0.2 mM vanadate and then 1 mM ATP. Stereo pair. Head-to-head linkers are seen to advantage. × 480,000. Fig. 17. Relaxed *Chlamydomonas* axoneme, unfixed, incubated in 1 mM ATP. Note how this "ATP image" is indistinguishable from the "vanadate image" of Fig. 16. × 480,000.

Figs. 12–22 show replicas of *Tetrahymena* and *Chlamydomonas* axonemes in the relaxed configuration. Some have been preincubated in ATP plus vanadate, whereas others have only been exposed to ATP; specific designations are given in the figure legends. Figs. 24 and 25 provide a direct comparison between rigor and relaxed arms at equivalent magnification. All but Figs. 18 and 19 were frozen without chemical fixation. Each of the five above-listed features of the relaxed arm is illustrated in these replicas from various perspectives.

DETACHMENT OF THE HEAD FROM THE D-FOOT: We noted that in rigor axonemes, the head occasionally associates with only one foot, and this is always the D-foot (e.g., Fig. 6, arrow). In ATP or ATP plus vanadate axonemes, by contrast, the head invariably associates with only one foot, and this is always the P-foot (Figs. 12–19). Hence ATP would appear to cause the head to shift its affinity from the D-foot to the P-foot. Because the rigor shift and the relaxed shift both convert the head from an elliptical profile to a round profile (see below), both appear to entail a rotation of the mallet-shaped head.

ROTATION OF THE HEAD: Four observations indicate that the relaxed head rotates downwards as it shifts its association to the P-foot. (*a*) The head acquires a circular profile in aerial view, averaging 13 nm in diameter (Figs. 12–19). (*b*) Arms seen in "horizon view," as in the right-hand row of Fig. 25, display only one protuberance over the P-foot whereas two protuberances are seen in comparable rigor images (Fig. 6, right-hand row). (*c*) In longitudinal fractures through inter-doublet gaps, the head is found to be disposed perpendicular to the axis of the microtubules rather than at the slewed angle characteristic of rigor (see also reference 72). (*d*) In cross- and oblique fracture (Figs. 20–22), the head extends farther down into the inter-doublet gap than it does in rigor (Fig. 3).

SHIFTS IN THE STALK POSITION: A diagnostic difference between rigor and relaxed arms is that the rigor stalk appears to attach to the head close to its proximal edge (Figs. 12–19, 25). Such a shift in position would occur if the stalk remained attached eccentrically to the head and the head rotated downward; therefore, it is not necessary to propose a displacement in the stalk attachment site *per se*. The angle made by a stalk as it crosses the interdoublet gap varies from a distinct tilt (up to 20° from the perpendicular) for some relaxed arms (e.g. Fig. 13) to a near perpendicular for others (e.g., Figs. 12 and 25), with some rows displaying a variety of stalk angles (e.g., Figure 15). As in rigor, some stalks associate with B protofilaments deep in the interdoublet space while others attach at higher positions (Figs. 16 and 25).

HEAD-TO-HEAD LINKS: Whereas inter-dynein linkers are difficult to discern in rigor, they form conspicuous head-to-head connections in the presence of ATP or vanadate plus ATP. In side view (Figs. 16, 17, and 25) they resemble spans on a suspension bridge, linking the heads at about their midlines. In frontal views (Figs. 13–15) they appear as wedges or snouts, their wide ends abutting on the more proximal heads and their tapered ends contacting the more distal heads. Fig. 23 diagrams how the rigor image of the linker can be converted to the relaxed image by postulating head rotation plus a shift in attachment of the linker from the P-foot to the basal aspect of the head.

P-FOOT EXTENSION: As noted earlier, the P-foot tends to be less prominent than the D-foot in rigor *Tetrahymena* (Fig. 9). In relaxed *Tetrahymena*, this tendency becomes the rule. Indeed, the P-foot often appears to detach from the A microtubule altogether and swing into the inter-doublet gap so that it forms an "elbow" between the D-foot and the head (Figs. 14, 15, and 25). In such cases, the angle from the perpendicular made by a line passing through the D-foot, P-foot, and head ranges from 30–39° with a mean of 32°; hence the arms display a dramatic tilt which sometimes is, and sometimes is not, accompanied by a similar tilt of their stalks.

In *Chlamydomonas*, on the other hand, the rigor P-foot tends to be coplanar or slightly prominent relative to the D-foot (Fig. 10), and in ATP the P-foot is invariably the more prominent of the two (Figs. 12, 16, and 17). Still, it is the P-foot that appears to detach from the A microtubule and swing toward the interdoublet gap in ATP, but at its most extreme (Figs. 16 and 17), the overall tilt of the arm remains modest by comparison with *Tetrahymena*.

Fixed versus Unfixed Relaxed Axonemes

The axonemes considered in the previous paragraphs derived from unfixed specimens (Figs. 12–17, 25). Relaxed axonemes fixed in glutaraldehyde plus ATP (Figs. 18 and 19) are in general comparable to their unfixed counterparts. The one persistent difference is that the arms are more irregularly disposed after fixation. Specifically, when a micrograph of a fixed axoneme is held perpendicular to one eye and the viewer sights along a row of arms, the position of the heads is often seen to shift erratically, recalling the distribution of piano-key hammers during a fugue (Figs. 18 and 19). By contrast, the

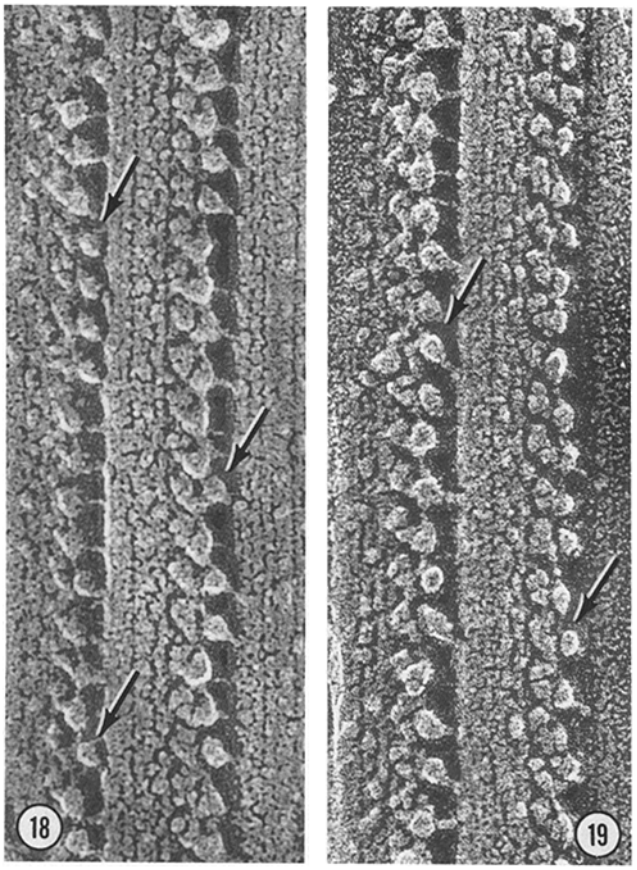

FIGURES 18 and 19 Two relaxed *Tetrahymena* axonemes, incubated in 0.5 mM ATP and then fixed in 1% glutaraldehyde in 0.5 mM ATP. Arrows in the left-hand row of Fig. 18 point out heads that appear to contact the B; other examples of displaced heads can be detected in other rows. × 255,000 and × 210,000.

position of the heads is remarkably uniform in most unfixed relaxed samples (e.g., Figs. 12–19), as well as in both fixed and unfixed rigor samples (Figs. 4–10). In *Chlamydomonas*, fixation so distorts the configuration of ATP-relaxed arms that the images become difficult to interpret (our unpublished data). These observations are consistent with the notion that the outer arms are less rigidly anchored to the axoneme in ATP than in rigor.

Rate and Reversibility of Arm Relaxation

When rigor axonemes are exposed to 1% glutaraldehyde containing 1 mM ATP, most of the arms in the resultant replicas are found to be in the relaxed configuration. Thus the rigor-to-relaxed shift occurs before there has been time for chemical crosslinking, presumably within seconds. Conversely, when axonemes are exposed to ATP and then washed free of

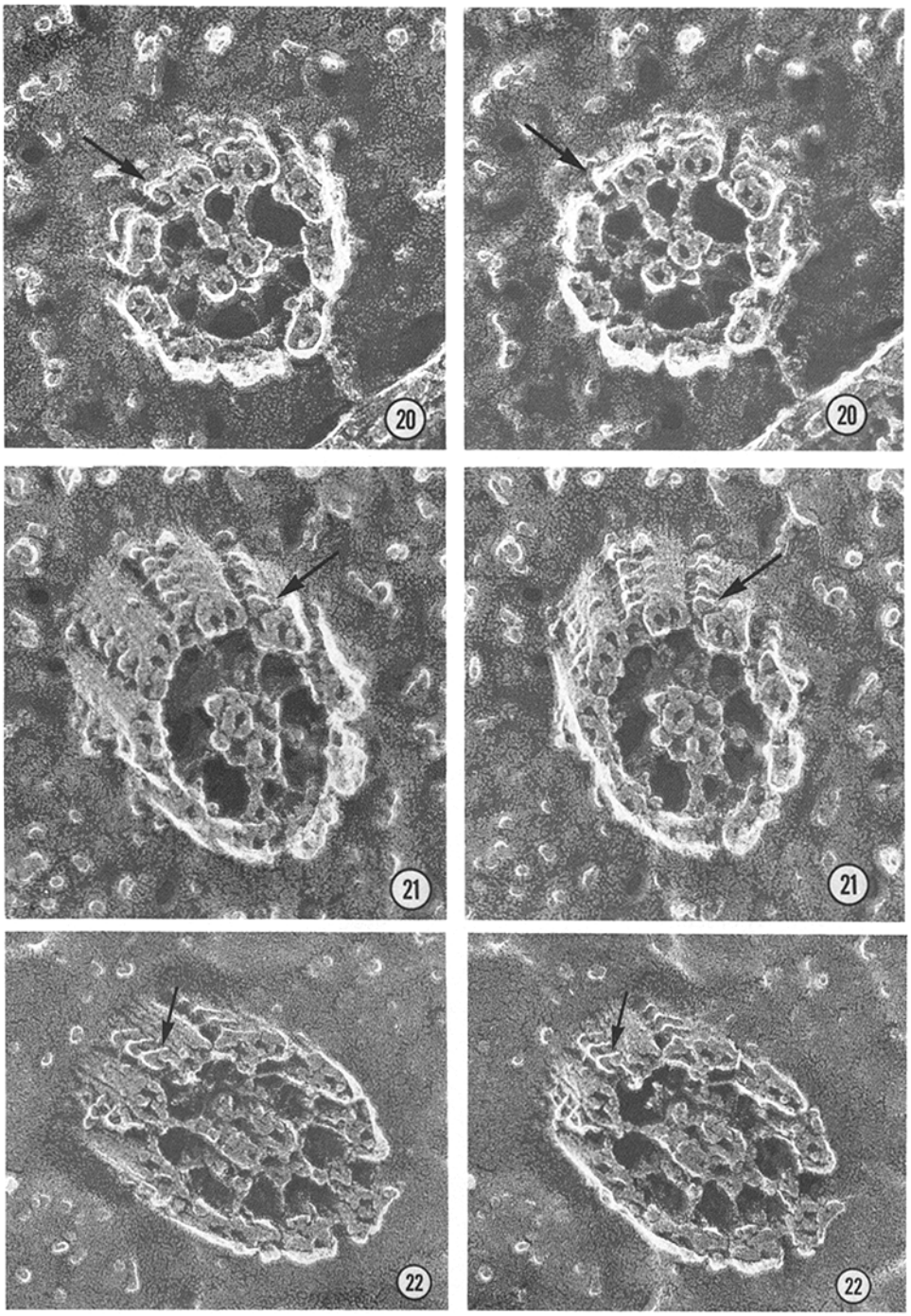

FIGURES 20–22 Three relaxed axonemes in cross-section, each incubated in vanadate plus ATP, unfixed, stereo pairs. Figs. 20 and 21 show *Chlamydomonas*; Fig. 22 shows *Tetrahymena*. Each is oriented as viewed from the tip to base, with the A microtubule to the left of the B in each doublet. Arrows denote arms that show to advantage the extension of the head down into the inter-doublet space. The more pronounced tilt of the *Tetrahymena* arms relative to the *Chlamydomonas* arms is evident. Contact of the radial spokes to the central sheath *via* their spoke heads is particularly evident in stereo. All × 200,000.

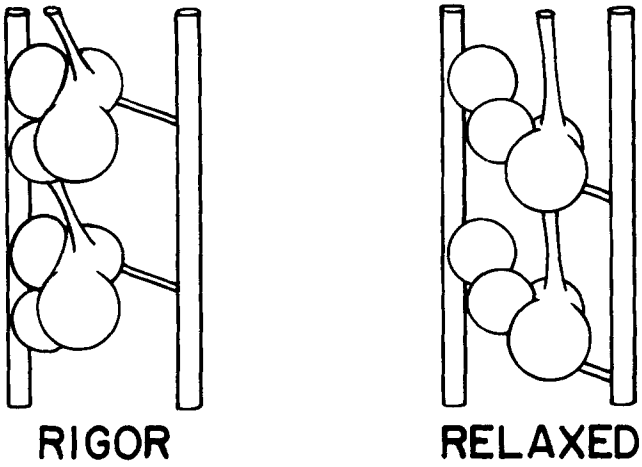

FIGURE 23 Aerial view diagram of the linker position in rigor and relaxed outer dynein arms. In rigor the linker extends down towards the adjacent P foot; in ATP it shifts up to make contact with the adjacent head, perhaps as a consequence of head rotation. Outer-arm components as in Figs. 2 and 11.

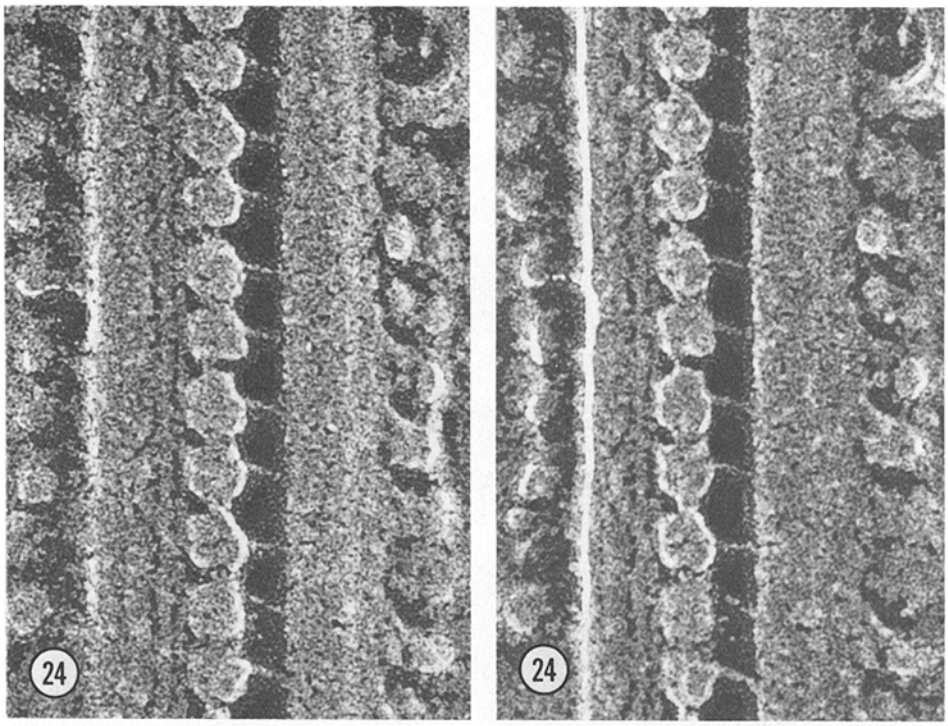

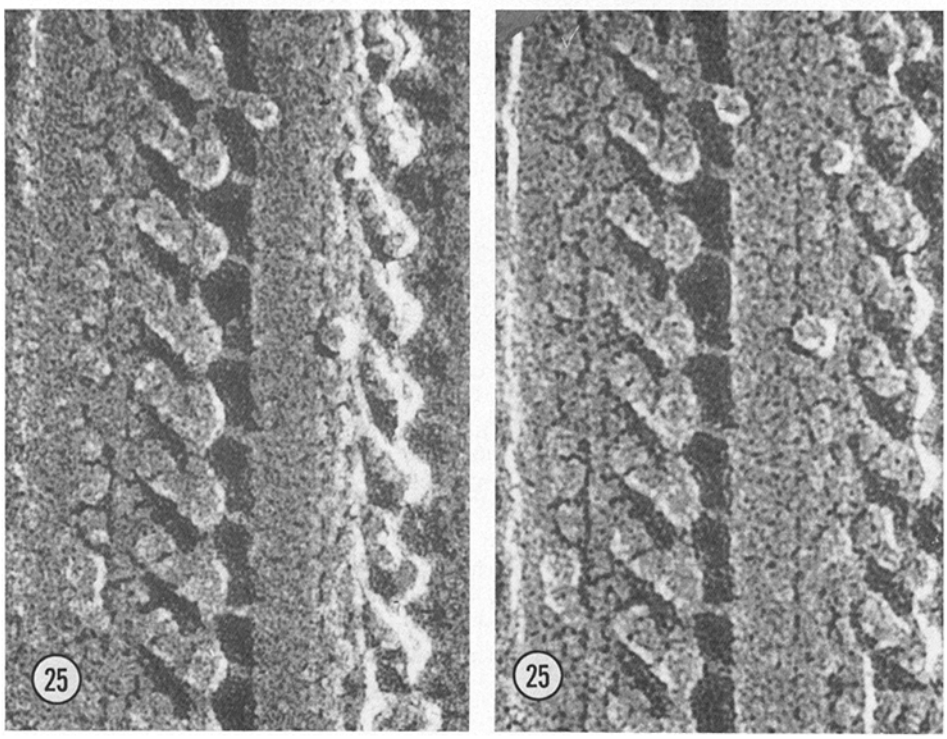

FIGURES 24 and 25 Rigor *versus* relaxed *Tetrahymena* axonemes, unfixed, stereo pairs. The relaxed axoneme (Fig. 25) was incubated in 0.1 mM vanadate and then 0.5 mM ATP. The heads obscure most of the feet in rigor, whereas the feet are clearly visible in the relaxed image. Shifts in head, stalk, and linker disposition are also apparent. × 400,000 and × 480,000.

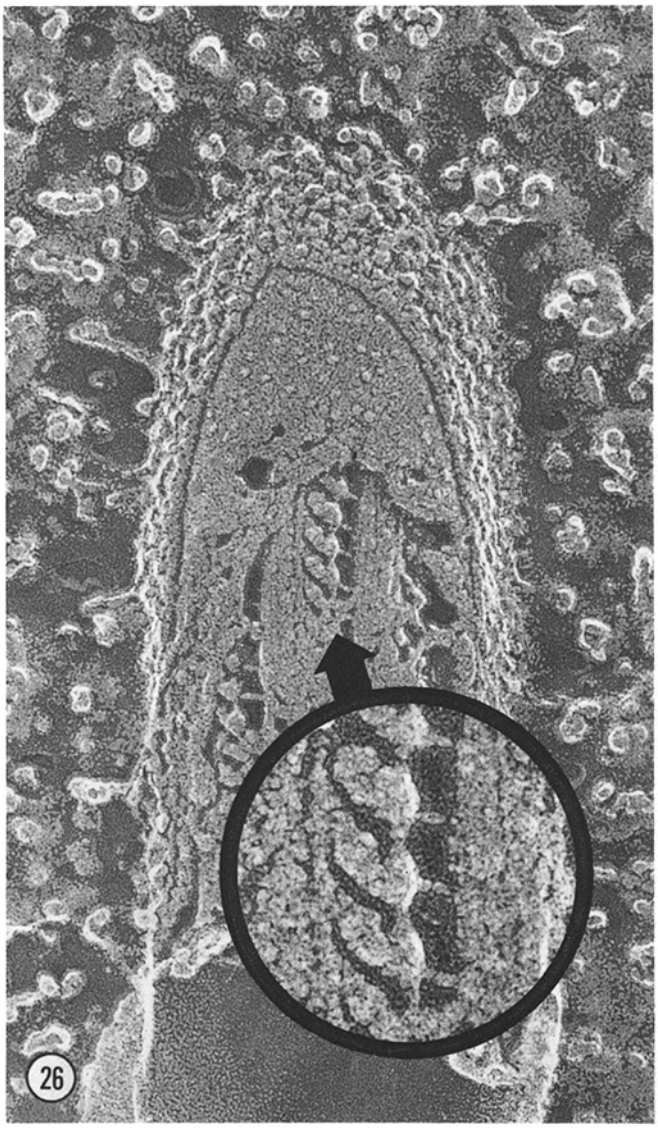

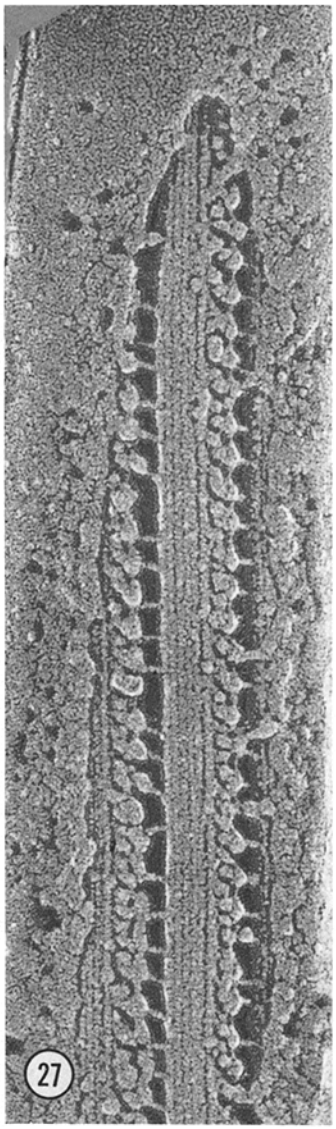

FIGURES 26 and 27 Fig. 26. Intact *Tetrahymena* cilium, unfixed, frozen while still attached to the cell. The exposed true surface of the ciliary membrane has a bumpy texture; the E fracture face beneath it carries scattered intramembranous particles. Exposed internally are two rows of relaxed outer dynein arms. The inset shows the upper row at higher magnification to allow direct comparison with Fig. 25. × 190,000. *Inset,* × 480,000. Fig. 27. Intact *Tetrahymena* cilium, unfixed, frozen while still attached to the cell. Membrane E fracture face is interrupted to reveal two rows of outer dynein arms. Relaxed configuration is particularly evident in the upper right-hand row. × 190,000.

ATP, they revert quantitatively to the rigor state. Therefore, the conformational changes described above are both rapid and reversible.

Outer Arms in Living Cilia

Figs. 26 and 27 show fortuitous fractures through the interiors of intact *Tetrahymena* cilia, attached to living cells, that were beating normally at the moment of freezing. All the outer arms are seen to be in the relaxed configuration, with the feet, heads, stalks, and linkers indistinguishable from their counterparts in axonemes exposed to ATP in vitro (compare the inset to Fig. 26 with Fig. 25).

Functional Attachment of Stalks

Our replicas indicate that stalks attach to the B tubule in rigor, in ATP, in ATP plus vanadate, and in the living state, yet many investigators have demonstrated that rigor axonemes are inflexible, whereas axonemes treated with ATP or ATP plus vanadate are very pliable (see *Discussion*). This suggests that the stalks attach much more firmly to the B tubule in rigor than in relaxed axonemes. To test this deduction, axonemes were squirted through a 27-gauge needle, fixed, and examined by deep-etch electron microscopy. The rigor axonemes proved to be very sturdily lashed together: even after 50 passages through the needle, when enough shear had been generated to snap many of the axonemes across their shafts, the doublets retained their 9 + 2 array and the stalks remained associated with the B microtubules. By contrast, several passages through the needle was sufficient to shear the ATP- or ATP plus vanadate-treated axonemes into individual doublets and central pairs, the arms associating quantitatively with the A microtubules. Interestingly, the vanadate-treated samples were far more extensively disrupted by the mechanical shear than were those beating in ATP, consistent with the concept that a proportion of the arms in beating axonemes are engaged in stronger, force-generating interactions.

A particularly informative image of the shearing process is shown in Fig. 28, where an unfixed, ATP-treated *Tetrahymena* axoneme was exposed to the air-water interface of an axonemal droplet moments before freezing. The shear forces present at the droplet interface have caused several doublets to "unzipper" at the level of the stalks, leaving the head, feet, and linkers attached to the A. Although it remains unclear whether the stalks detach at their "B ends" or their "head ends," it is clear that they constitute the weak link in the system. We conclude, therefore, that the stalks form strong associations with the B microtubule during rigor, whereas in ATP and

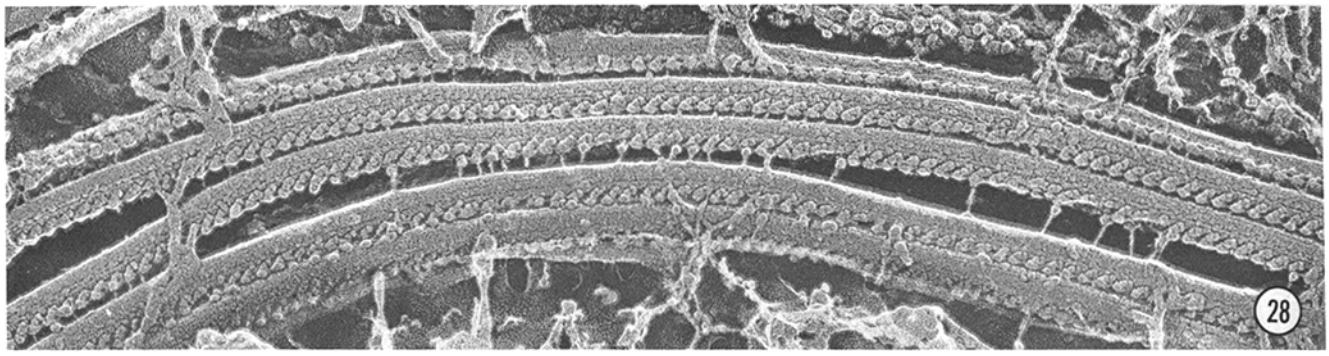

FIGURE 28 Relaxed *Tetrahymena* cilium, unfixed, incubated in 0.5 mM ATP, and located just at the air-water interface of the axoneme suspension at the time of freezing. Arms are tearing or torn away from their B attachment sites at several locations. In regions of tear, the stalks stretch to several times their normal length. In torn regions, heads, feet, and linkers all remain associated with the A. Note that the stalks are obscured in regions where the doublets have been artifactually compressed (see Materials and Methods). × 94,000.

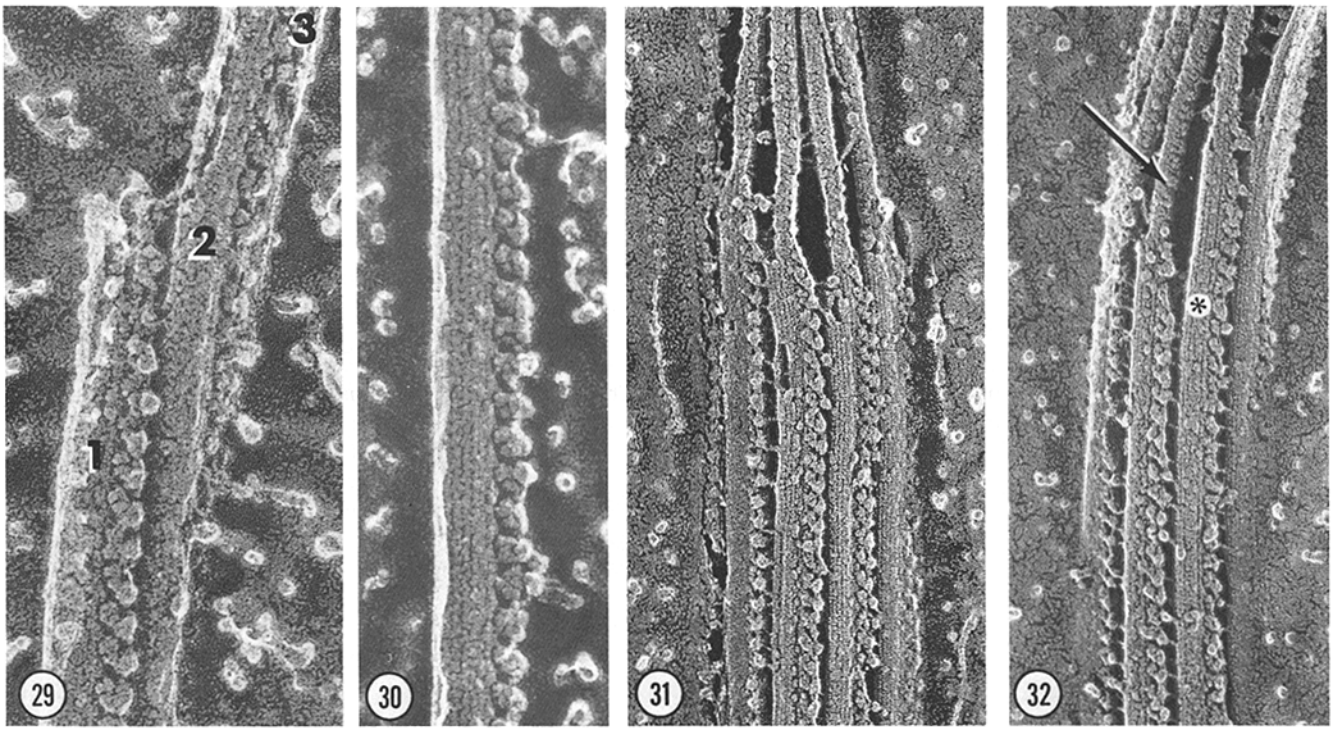

FIGURES 29–32 Fig. 29. Three doublets (*1–3*) of a *Tetrahymena* axoneme, prepared by Protocol B (see Materials and Methods), undergoing sliding disintegration in response to 0.1 mM ATP. Glutaraldehyde-fixed. Arms associated with the A microtubule are in the relaxed configuration. × 215,000. Fig. 30. Doublet from *Tetrahymena*, prepared by Protocol B (see Materials and Methods), that has undergone sliding disintegration in response to 0.1 mM ATP. Glutaraldehyde-fixed. Arms associate with the A microtubule and retain a relaxed configuration. × 215,000. FIGURES 31 and 32 *Tetrahymena* axonemal tips, unfixed, showing relative sliding of doublets. See text for details. × 115,000.

particularly in ATP plus vanadate they are more loosely attached.

Inter-doublet Sliding

The current version of the sliding-filament model of ciliary motility (53) holds that during the active stroke, the outer dynein arms make reversible contacts with B microtubules such that the B of one doublet is pushed tipwards past the A of its adjacent doublet. Major support for this concept derives from "sliding-disintegration" experiments. Summers and Gibbons (62) and Sale and Satir (52) have shown that when protease-treated axonemes are exposed to ATP, the doublets slide past one another in a telescoping fashion, leaving the arms associated with the A tubules.

Fig. 29 shows a replica of three *Tetrahymena* doublets in the act of sliding disintegration, and Fig. 30 shows a fully "slid" doublet. The head, feet, and linker components clearly remain associated with the A microtubules during and following sliding disintegration. Because we are unable to visualize the stalk, we do not know whether it falls off the arm, falls back on the head, or falls back on the apparently naked B. Even after sliding, the arms retain their relaxed configuration (Fig. 30), with heads rotated and displaced basally and linkers connecting adjacent heads.

A more natural view of the sliding process is provided by

Figs. 31 and 32. Shown are two *Tetrahymena* axonemal tips, readily identified as such by the termination of the B microtubules (53) and by the presence on the singlet A microtubules of a mottled material, disposed as a left-handed helix, which either covers or replaces the usual protofilament organization. Both axonemes were exposed to ATP and their outer arms are in the relaxed configuration. The singlet A microtubules are straight in Fig. 31, whereas they curve to the right in Fig. 32. In Fig. 31, all the arms terminate at about the same level as the B microtubules, their expected disposition when the tip of the cilium is straight (53). As the tip curves to the right (Fig. 32), the terminal portion of the doublet on the inside of the curve (asterisk) extends past its neighboring doublet so that its B microtubule comes to face its neighbor's singlet A microtubule (arrow). In this region, the B microtubule is "naked": the head, feet, and linkers that associated with it in the straight configuration remain behind, associated with the A microtubule of the neighboring doublet. The sliding doublet is seen to have moved relative to its neighbor by ~144 nm (six outer-arms worth). Because recent estimates predict that doublets should slide a maximum of 140 nm relative to one another during the native beat (12), this image strongly supports some of the basic tenets of the sliding filament model.

DISCUSSION

Outer Arm Substructure

Using the quick-freeze deep-etch technique, the outer dynein arms of *Teterahymena* and *Chlamydomonas* are found to be composed of five morphologically distinct components that we denote as a proximal and a distal foot, a head, a stalk, and an inter-dynein linker. Details of their structure are illustrated in Figs. 1, 2, 11, and 23 and will not be reiterated here. All of these components are removed from the axoneme during high-salt extraction (33) (our unpublished data), and all are absent from the outer arm-defective mutants of *Chlamydomas, pf-13a* and *pf-22* (30) (our unpublished studies with Dr. Bessie Huang, Baylor School of Medicine). Therefore, all five appear to be *bona fide* constituents of the outer dynein arm as traditionally defined.

We have, in addition, examined replicas of rigor axonemes from sea urchin sperm flagella (prepared by Dr. Winfield Sale, Emory University), mussel gill cilia, mouse trachea cilia, human nasal cilia (prepared by Dr. Charles Kuhn, Washington University), trypanosome flagella (prepared by Dr. Wanderley de Souza, University of Rio de Janeiro) and several protozoa resident in the termite gut and in pond water. In all cases we find the same basic outer-arm substructure as described here for *Tetrahymena* and *Chlamydomonas.* Therefore, dynein morphology appears to be a highly conserved feature of the eukaryotes.

Several previous studies have concluded that outer dynein arms are composed of subunits. Outer arms have been described as linear polymers of three similar subunits in negatively stained axonemes (54, 69), and isolated dynein has been described as forming either long linear aggregates of 9 × 14 nm particles (19), shorter aggregates of particles that measure 10–12 nm in diameter (70), or bouquets of three particles on three connected strands (32). A recent study (75) described isolated outer arms as heart-shaped structures, 20 × 25 nm, with two "heads" opposite a pointed end; it is difficult to determine whether these "heads" correspond to the bifurcated outer-arm heads described here or to the feet. Lacking in all these studies has been the 3-D perspective provided by the deep-etch replicas, which greatly simplifies the task of identifying individual components and their spatial relationships to one another.

Our approach has revealed that whereas outer arms are roughly perpendicular to the long axis of the axonemes in rigor, ATP induces them to undergo a distinct basal tilt. The observations of Witman and Minervini (72) support this conclusion, but earlier negative-stain and thin-section studies are conflicting. Warner and Mitchell (69) concluded that outer arms are tilted (some 32° from the perpendicular) both in rigor and in ATP-exposed axonemes; Takahashi and Tonomura (63) stated that the arms are even more tilted in rigor than in ATP (35° vs. 29°); and Haimo et al. (23) and Satir et al. (55) also reported that the arms are tilted (35–40°) in rigor. We have no explanation for these discrepancies.

In any case, our replicas illustrate quite clearly that a critical event induced by ATP is the dissociation of the outer-arm head from the D-foot. This change may relate to the shift from a "latant" to a "nonlatant" state of the dynein ATPase that is stimulated by low-salt conditions and by agents that disturb hydrophobic interactions (4, 11, 14, 18, 64), since several of these treatments have been shown to cause a conformational change in isolated outer arms (5) and to dissociate them into particles with a lower sedimentation velocity (18, 64).

Individual Outer Arm Components

Each of the individual outer-arm components identified in this study can, in retrospect, be visualized in certain previously published electron micrographs. Moreover, several of the known properties of dynein arms can be explained in terms of the components described here.

The stalk is most clearly visible in the *Paramecium* cilium shown in Fig. 15 of Plattner et al. (50), although it is not identified as such. (Also visible in their Fig. 15 is a second set of stalks, closer to the membrane, which we fail to detect in *Tetrahymena.*) In the micrographs of redecorated microtubules by Haimo et al. (23), moreover, faint strands are present in the expected position of stalks, suggesting that the stalks are retained by isolated outer dynein arms and participate in microtubule cross-bridging in vitro.

We have considered carefully the possibility that the stalks are synonymous with nexin links (reviewed in reference 37), but this does not appear to be the case. Nexin links are defined as spanning microtubules in the axoneme interior, whereas the stalks are located at the axoneme exterior. The nexin links are 30-nm long and repeat with a 96-nm period, whereas the stalks are 11-nm long and repeat with a 24-nm period. Finally, the nexin links are reported to persist after high-salt extraction (49) and in the outer arm-less mutants of *Chlamydomonas* (30), whereas the stalks are absent in both cases. Because the inner dynein arms are also head-and-stalk structures (our unpublished data), it is possible that either or both sets of stalks have been interpreted as nexin in certain studies.

The feet are of interest because certain persons with Kartagener's syndrome, an inherited immotile cilia condition (1), bear cilia with short protuberances on each A microtubule in the location expected for the outer-arm feet (57, 60), but lack the bulky components we have described as head, stalk, and linker.

The inter-dynein linkers are evident in Fig. 9*a* of Warner and Mitchell (69) and in Fig. 4 of Mitchell and Warner (44); we suspect that they also correspond to the flared material observed in isolated dynein arms (23). They are clearly com-

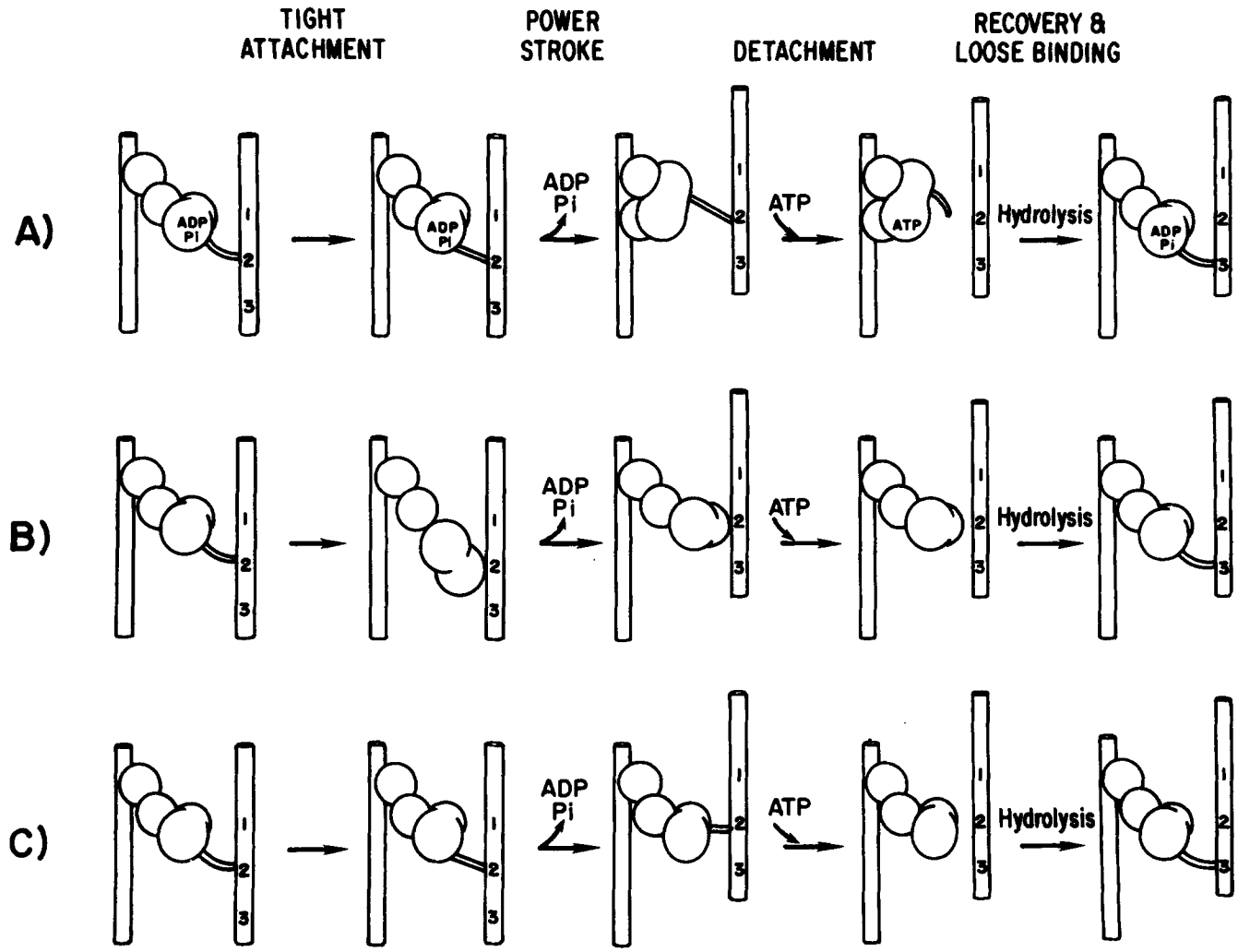

FIGURE 33 Three models of the dynein arm cycle suggested by the observations reported in this paper. For each panel, the A microtubule of one doublet is on the left; the B microtubule of its neighboring doublet is on the right, with three of its hypothetical binding positions numbered. In each model, the cycle begins and ends with the arm in a relaxed, product-release configuration, in which it is only loosely associated with the B tubule (symbolized by a curved stalk). (*A*) Model assuming that the rigor configuration is adopted during the force-generating phase of the cycle, based on the Lymn and Taylor paradigm (40) for the myosin ATPase cycle. The stalk is first stimulated to associate more tightly to the B microtubule; tight binding stimulates the release of nucleotide products and a shift of the head into the rigor configuration, which pulls the B tubule upwards in the process (see Fig. 34 for a dynamic view of this "power stroke"); in the rigor conformation the arm is able to bind another ATP and detach from the B tubule; it then shifts downwards to reattach loosely at the next site as the ATP is hydrolyzed. (B) Model assuming that the stalk does not function during the force-generating phase of the cycle, but rather serves to keep the head away from the B during relaxation. When the stalk is stimulated to swing aside, the head moves out and makes direct contact with the B; the whole arm then flexes, translating the contiguous doublet distally, much as in previous models of dynein arm activity (51, 54). (*C*) Model assuming that the rigor configuration *per se* is not adopted during the cycle but retaining the notion that the stalks play an active role in force generation, functioning as tiny stilts that undergo fine movements analogous to the overall arm changes proposed in Model A. The stalk is first stimulated to bind tightly to the B; it then shifts from an extended to a flexed conformation, either an an autonomous change or one caused by a swiveling of the head, translocating the contiguous doublet distally.

parable to the spur-shaped units described in negatively stained axonemes of *Chlamydomonas* (72), and may explain the tendency of isolated arms to behave as aggregates (19, 22, 63, 64). If, as it appears, all the outer dynein arms in a row are physically linked together, particularly in the presence of ATP, this arrangement has obvious implications both for the assembly/disassembly of the axoneme and for the transmission of activation signals and/or mechanical forces along the axoneme.

Outer-arm Conformations in Nonmotile Cilia

Axonemes can be rendered nonmotile under two experimental conditions: they can be depleted of ATP, whereupon the arms assume the locked, perpendicular configuration we denote as rigor, or they can be incubated in the presence of ATP plus vanadate, whereupon the arms assume the open, tilted configuration we denote as relaxed. We review below the reported effects of ATP depletion and of ATP plus vanadate treatment on the physical and enzymatic properties of axonemes, and then relate these studies to our morphological observations.

Micromanipulation studies have demonstrated that whereas rigor axonemes are stiff and inflexible (10, 46), much as rigor muscle fibers, axonemes incubated in ATP plus vanadate are pliant and deformable (45, 46), a state often denoted as "relaxed." These observations have suggested that the outer dynein arms are "attached" in rigor and "detached" in relax-

ation (51), as is thought to be the case for myosin crossbridges in striated muscle.

Enzymatic studies of dynein (45, 47, 58) and other ATPases (20, 41) have concluded that vanadate does not prevent either the ATP binding or ATP hydrolysis steps of the ATPase cycle. However, an ADP·V complex forms that cannot be released from the enzyme, preventing further rounds of hydrolysis. The dynein·ADP·V complex is believed to be equivalent to the dynein·ADP·P complex that forms during the native cycle. Release of the ADP and phosphate products from the enzyme has been found in kinetic studies (31) to be the slowest step in the cycle, as has been found with myosin ATPase (40).

Taken together, these studies predict that dynein outer arms incubated in ATP plus vanadate should be trapped in the product-release stage of their cycle, and that this should cause them to become functionally detached from the B microtubules so that the axoneme becomes pliant. Our images present an apparent dilemma, therefore, in that we find that the outer arm stalks bridge adjacent doublets in both rigor ("attached") and vanadate-inhibited ("detached") conditions. To resolve the dilemma, it might be suggested that the tilted arms are in fact "hinged," capable of swiveling at an elbow created by the D-foot/P-foot junction and/or the P-foot/head junction. However, such a hinge would only allow adjacent doublets to shift a few nanometers relative to one another, whereas the large passive bends induced by micromanipulation of relaxed axonemes would presumably require some 100 nm of interdoublet sliding. We are therefore led to propose that in the rigor state, the stalks attach firmly to the B microtubules and help to prevent interdoublet sliding, whereas in the relaxed state, the stalks attach only weakly to the B microtubules and are free to slide up and down them. Supporting this proposal is our observation that relaxed but not rigor axonemes are easily ripped apart by hydrodynamic shear. It is important to stress that the physical properties of rigor and relaxed axonemes are probably *also* determined by additional components of the axoneme (inner arms, radial spokes, nexin links, etc.).

Outer Arm Configuration in Beating Cilia

We find that the overwhelming majority of outer dynein arms in both beating axonemes and in living motile cilia are in a tilted configuration that is indistinguishable from the tilted configuration adopted in ATP plus vanadate. Based on the reasoning followed above, therefore, we conclude that most of the arms in beating cilia must be poised in the product-release stage of their cycle, functionally detached from their adjacent doublets. This conclusion is supported by the ciliary beat pattern itself, which suggests that local regions of bend formation and propagation occur within an organelle that is otherwise relatively inactive and pliant. It is also supported by micromanipulation studies (10, 39, 46) and by our hydrodynamic shear experiments, which indicate that beating cilia are readily dissociable compared with rigor cilia.

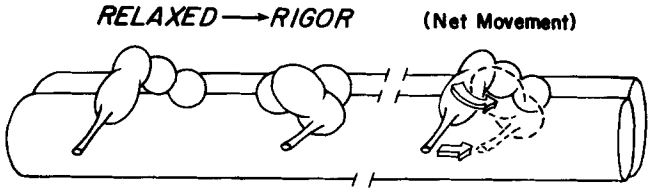

FIGURE 34 Diagram of the "power stroke" postulated in Fig. 33 *A*. The viewer is facing the side of an A microtubule, seeing the arms from the perspective of the neighboring B microtubule. Binding of the stalk to the B tubule initiates an internal flexion in the arm that brings its head into contact with its D-foot, i.e., into the rigor configuration. The flexion shifts the stalk-attachment point distally by ~8 nm; hence the B microtubule is displaced relative to the A by ~8 nm.

The Generation of Force

We are left, then, with the critical question: what is the configuration of the outer arm during the active, force-generating phase of its cycle? We have already explained why it is probable that at any moment, most of the arms in a beating cilium are not even stimulated to undergo these changes and remain in the relaxed configuration. Moreover, the few arms in a bending region that are induced to carry out their ATPase cycle would still be expected to spend the longest time in the product-release configuration (31), which also looks relaxed. Therefore, we predict that in a population of beating cilia, very few outer arms will be caught in some other, force-generating configuration. Unfortunately, a morphologist, in distinguishing truth from artifact, relies heavily on visualizing a structural feature repeatedly and predictably; hence transient and infrequent configurations are most refractory to identification, and we cannot yet claim to have identified these critical intermediates.

Nevertheless, the most obvious possibility is that the force-generating cycle includes the rigor conformation that we visualize after ATP depletion, an idea also central to most models of striated muscle contraction. A scheme incorporating this suggestion is drawn in Figs. 33*A* and 34, with details given in the legends. Although we presently favor this model, we have not yet obtained micrographs showing arms in a clear-cut rigor configuration in curved regions of beating axonemes. Therefore, we have also entertained two other possible models for the force-generating state, drawn in Fig. 33*B* and *C* and detailed in the legend. We should note that it is also conceivable that the stalks are permanently attached to both the B tubule and the heads and that the heads cyclically attach and detach from the feet during the ciliary beat. Although the "ping-pong" images in glutaraldehyde-fixed preparations (Figs. 18 and 19) support this suggestion, it predicts that interdoublet sliding should generate A microtubules bearing feet and B microtubules bearing heads and stalks, and this is not observed (Figs. 29–32).

Coupling Dynein ATPase Activity to Bend Formation

Most models of ciliary motility (16) assume that the sequential activation of dynein arms to produce up to 60–80 beats per second is not accomplished by diffusion of ATP or ions. Instead, it is assumed that axonemes are bathed in a relatively constant chemical environment, much as they are during in vitro beating, and that sequential outer-arm activation is stimulated by some other mechanism. The mechanism most favored by theoreticians is a curvature-control mechanism (7; reviewed in reference 6) wherein the ATPase activity of the outer arms, and hence their force-generating capacity, is sensitive to the degree of axonemal bending.

Our images of outer dynein arms permit us to formulate a more specific proposal as to how curvature control might operate. Protofilaments in an axonemal doublet will undoubtedly experience different degrees of "strain," depending on their relative locations with respect to a particular bend. Spe-

cifically, those protofilaments on the outside of a curve will be "stretched" and those on the inside "compressed" relative to protofilaments located on the sides of a bend or in unbent regions of the axoneme. Such differences are likely to affect the disposition of the tubulin subunits within each protofilament (9, 34). In this case, one could imagine that tubulin dimers in a normal or compressed lattice expose only weak binding sites to the dynein stalks (sites so weak that the stalks can easily jump from one to the next), whereas tubulin dimers in a stretched lattice expose strong binding sites to the stalks (sites strong enough to transmit forces generated by ATP hydrolysis and outer arm movements). Furthermore, the strong binding could stimulate product release from the dynein ATPase in the same fashion that tight actin binding appears to stimulate product release from the myosin ATPase (59), and thus perpetuate the cycle.

These ideas are consistent with the observation that tubulin can stimulate dynein ATPase activity in vitro (29), and with the observation that short, broken pieces of doublets, presumably refractory to bend, stimulate dynein ATPase activity much less well than intact doublets (8). However, the critical assumption is that the tubulin lattice changes during the course of bend formation. Since we can visualize tubulin lattices directly in favorable platinum replicas (27), this assumption can be put to test.

Ms. Robyn Carmody prepared all of the deep-etch replicas presented in this paper; her skillful and efficient expertise cannot be overpraised. Dr. Meng-Chao Yao and Ms. Carol Hwang kindly provided the *Tetrahymena* and *Chlamydomonas* cultures. Special thanks go to Drs. Leah Haimo, Win Sale, and George Witman for their helpful advice on technical procedures. Thanks also to Marilyn Zimmerman for preparing the final figures, Jan Wuelling for preparing the manuscript, and Anne Dillon for the drawings.

This work was supported by grants from the National Institutes of Health to U. W. Goodenough and J. E. Heuser.

Received for publication 7 May 1982, and in revised form 31 August 1982.

REFERENCES

1. Afzelius, B. A. 1976. A human syndrome caused by immotile cilia. (*Science Wash. D. C.*) 193:317–319.
2. Allen, R. D. 1968. A reinvestigation of cross-sections of cilia. *J. Cell Biol.* 37:825–831.
3. Amos, L. A., R. W. Linck, and A. Klug. 1976. Molecular structure of flagellar microtubules. *In* Cell Motility. R. Goldman, T. Pollard, and J. Rosenbaum, editors. Cold Spring Harbor Laboratory, Cold Spring Harbor, NY. 847–868.
4. Blum, J. J., and A. Hayes. 1978. Effects of sulfhydryl reagents on the ATPase activity of solubilized 14S and 30S dyneins and on whole ciliary axonemes as a function of pH. *J. Supramol. Struct.* 8:153–171.
5. Blum, J. J., A. Hayes, C. C. Whisnaut, and G. Rosen. 1977. Effect of spin-labeled maleimide on 14S and 30S dyneins in solution and on demembranated ciliary axonemes. *Biochemistry.* 16:1937–1943.
6. Blum, J. J., and M. Hines. 1979. Biophysics of flagellar motility. *Q. Rev. Biophys.* 12:103–180.
7. Brokaw, C. J. 1971. Bend propagation by a sliding filament model for flagella. *J. Exp. Biol.* 55:289–304.
8. Brokaw, C. J., and B. Benedict. 1968. Mechanochemical coupling in flagella. I. Movement-dependent dephosphorylation of ATP by glycerinated spermatozoa. *Arch. Biochem. Biophys.* 125:770–778.
9. Douglas, G. J. 1975. Sliding filaments in sperm flagella. *J. Theor. Biol.* 53:247–252.
10. Gibbons, B. H., and I. R. Gibbons. 1974. Properties of flagellar "rigor waves" formed by abrupt removal of adenosine triphosphate from actively swimming sea urchin sperm. *J. Cell Biol.* 63:970–985.
11. Gibbons, B. H., and I. R. Gibbons. 1979. Relationship between the latent adenosine triphosphatase state of dynein 1 and its ability to recombine functionally with KCl-extracted sea urchin sperm flagella. *J. Biol. Chem.* 254:197–201.
12. Gibbons, B. H., and I. R. Gibbons. 1980. Calcium-induced quiescence in reactivated sea urchin sperm. *J. Cell Biol.* 84:13–27.
13. Gibbons, I. R. 1961. The relationship between the fine structure and the direction of beat in gill cilia of a lamellibranch mollusc. *J. Biophys. Biochem. Cytol.* 11:179–205.
14. Gibbons, I. R. 1965. Chemical dissection of cilia. *Arch. Biol.* 76:317–352.
15. Gibbons, I. R. 1975. The molecular basis of flagellar motility in sea urchin spermatozoa. *In* Molecules and Cell Movement. S. Inoue and R. E. Stephens, editors. Raven Press, New York. 207–232.
16. Gibbons, I. R. 1981. Cilia and flagella of eukaryotes. *J. Cell Biol.* 91:107s–124s.
17. Gibbons, I. R., M. P. Cosson, J. A. Evans, B. H. Gibbons, B. Houck, K. H. Martinson, W. S. Sale, and W. Y. Tang. 1978. Potent inhibition of dynein adenosine triphosphatase and of the motility of cilia and sperm flagella by vanadate. *Proc. Natl. Acad. Sci. U. S. A.* 75:2220–2224.
18. Gibbons, I. R., and E. Fronk. 1979. A latant adenosine triphosphatase form of dynein 1 from sea urchin sperm flagella. *J. Biol. Chem.* 254:187–196.
19. Gibbons, I. R., and A. J. Rowe. 1965. Dynein: a protein with adenosine triphosphatase activity from cilia. *Science (Wash. D. C.).* 149:424–426.
20. Goodno, C. C., and E. W. Taylor. 1982. Inhibition of actomyosin ATPase by vanadate. *Proc. Natl. Acad. Sci. U. S. A.* 79:21–25.
21. Gorovsky, M. A., M-C. Yao, J. B. Keevert, and G. L. Pleger. 1975. Isolation of micro- and macronuclei of *Tetrahymena pyriformis*. *Methods Cell Biol.* 9:311–327.
22. Haimo, L. T., and J. L. Rosenbaum. 1981. Dynein binding to microtubules containing microtubule-associated proteins. *Cell Motility* 1:499–515.
23. Haimo, L. T., B. R. Telzer, and J. L. Rosenbaum. 1979. Dynein binds to and cross-bridges cytoplasmic microtubules. *Proc. Natl. Acad. Sci. U. S. A.* 76:5759–5763.
24. Heuser, J. E. 1980. Three-dimensional visualization of coated vesicle formation in fibroblasts. *J. Cell Biol.* 84:560–583.
25. Heuser, J. E. 1981. 3-D visualization of biological samples that are quick-frozen, deep-etched and rotary-replicated. *In* 3-D Ultrastructure in Biology. J. Turner, editor. Academic Press, New York. 97–122.
26. Heuser, J. E. 1981. The quick-freeze, deep-etch method of preparing samples for high resolution, 3-D electron microscopy. *Trends Biochem. Sci.* 6:64–68.
27. Heuser, J. E., and M. W. Kirschner. 1980. Filament organization revealed in platinum replicas of freeze-dried cytoskeletons. *J. Cell Biol.* 86:212–234.
28. Heuser, J. E., T. S. Reese, L. Y. Jan, Y. N. Jan, M. J. Dennis, and L. Evans. 1979. Synaptic vesicle exocytosis captured by quick-freezing and correlated with quantal transmitter release. *J. Cell Biol.* 81:275–300.
29. Hoshino, M. 1976. Interactions of *Tetrahymena* dynein with microtubule protein. Tubulin-induced stimulation of dynein ATPase activity. *Biochim. Biophys. Acta.* 462:49–62.
30. Huang, B., G. Piperno, and D. J. L. Luck. 1979. Paralyzed flagella mutants of *Chlamydomonas reinhardtii* defective for axonemal doublet microtubule arms. *J. Biol. Chem.* 254:3091–3099.
31. Johnson, K. A., and M. E. Porter. 1982. Transient state kinetic analysis of the dynein ATPase. *Cell Motility Suppl. 1*:101–106.
32. Johnson, K. A., and J. S. Wall. 1982. The structure and molecular weight of 30S dynein from *Tetrahymena*. *Biophys. J.* 37:345a (Abstr.).
33. Kincaid, H. L., Jr., B. H. Gibbons, and I. R. Gibbons. 1973. The salt-extractable fraction of dynein from sea urchin sperm flagella: an analysis by gel electrophoresis and by adenosine triphosphatase activity. *J. Supramol. Struct.* 1:461–470.
34. Klug, A. 1967. The design of self-assembling systems of equal units. *In* Formation and Fate of Cellular Organelles. K. B. Warren, editor. Academic Press, New York. 1–18.
35. Kobayashi, T., T. Martensen, J. Nath, and M. Flavin. 1978. Inhibition of dynein ATPase by vanadate, and its possible use as a probe for the role of dynein in cytoplasmic motility. *Biochem. Biophys. Res. Commun.* 81:1313–1318.
36. Linck, R., D. Albertini, G. Langevin, G. Olson, and D. Woodrum. 1981. The structure and function of microtubules. *Biophys. J.* 33:215a (Abstr.).
37. Linck, R. W. 1979. Advances in the ultrastructural analysis of the sperm flagellar axoneme. *In* The Spermatozoan. D. W. Fawcett and J. M. Bedford, editors. Urban and Schwarzenberg, Baltimore, MD. 99–118.
38. Linck, R. W., D. F. Albertini, D. M. Kenney, G. L. Langevin, and A. W. Vogl. 1982. Evidence that intermediate-filament-like proteins form integral components of microtubules. *Biophys. J.* 37:346a (Abstr.).
39. Lindemann, C. B., W. G. Rudd, and R. Rikmenspoel. 1973. The stiffness of the flagella of impaled bull sperm. *Biophys. J.* 13:437–448.
40. Lymn, R. W., and E. W. Taylor. 1971. Mechanism of adenosine triphosphate hydrolysis by actomyosin. *Biochemistry.* 10:4617–4624.
41. Macara, I. G. 1980. Vanadium—an element in search of a role. *Trends Biochem. Sci.* 5:92–94.
42. Martin, N. C., and U. W. Goodenough. 1975. Gametic differentiation in *Chlamydomonas reinhardtii*. I. Production of gametes and their fine structure. *J. Cell Biol.* 67:587–605.
43. Miller, K. R., and N. L. Lassignal. 1981. Filament-like artifacts associated with rapid freezing and freeze-drying. *J. Cell Biol.* 91:304a (Abstr.).
44. Mitchell, D. R., and F. D. Warner. 1980. Interactions of dynein arms with B subfibers of *Tetrahymena* cilia: quantitation of the effects of magnesium and adenosine triphosphate. *J. Cell Biol.* 87:84–97.
45. Okuno, M. 1980. Inhibition and relaxation of sea urchin sperm flagella by vanadate. *J. Cell Biol.* 85:712–725.
46. Okuno, M., and Y. Hiramoto. 1979. Direct measurements of the stiffness of echinoderm sperm flagella. *J. Exp. Biol.* 79:235–243.
47. Penningroth, S. M., A. Cheung, K. Olehnik, and R. Koslosky. 1982. Mechanochemical coupling in the relaxation of rigor-wave sea urchin sperm flagella. *J. Cell Biol.* 92:733–741.
48. Pinto da Silva, P., and B. Kachar. 1980. Quick-freezing vs. chemical fixation: capture and identification of membrane fusion intermediates. *Cell Biol. Int. Rep.* 4:625–640.
49. Piperno, G., and D. J. L. Luck. 1979. Axonemal adenosine triphosphatases from flagella of *Chlamydomonas reinhardtii*. *J. Biol. Chem.* 254:3084–3090.
50. Plattner, H., C. Westphal, and R. Tiggemann. 1982. Cytoskeleton-secretory vesicle interactions during the docking of the secretory vesicles at the cell membrane in *Paramecium tetraurelia* cells. *J. Cell Biol.* 92:368–377.
51. Sale, W. S., and I. R. Gibbons. 1979. Study of the mechanism of vanadate inhibition of the dynein cross-bridge cycle in sea urchin sperm flagella. *J. Cell Biol.* 82:291–298.
52. Sale, W. S., and P. Satir. 1977. Direction of active sliding of microtubules in *Tetrahymena* cilia. *Proc. Natl. Acad. Sci. U. S. A.* 74:2045–2049.
53. Satir, P. 1968. Studies on cilia III. Further studies on the cilium tip and a "sliding filament" model of ciliary motility. *J. Cell Biol.* 39:77–94.
54. Satir, P. 1979. Basis of flagellar motility in spermatozoa: Current status. In The Spermatozoon. D. W. Fawcett and J. M. Bedford, editors. Urban and Schwarzenberg, Baltimore, MD. 81–90.
55. Satir, P., J. Wais-Steider, S. Lebduska, A. Nasr, and J. Avolio. 1981. The mechanochemical cycle of the dynein arm. *Cell Motility.* 1:303–327.
56. Schliwa, M., J. van Bierkom, and K. R. Porter. 1981. Stabilization of the cytoplasmic ground substance in detergent-opened cells and a structural biochemical analysis of its composition. *Proc. Natl. Acad. Sci. U. S. A.* 78:4329–4333.
57. Schneeberger, E. E., J. McCormack, H. J. Issenberg, S. R. Schuster, and P. S. Gerald. 1980. Heterogeneity of ciliary morphology in the immotile cilia syndrome in man. *J. Ultrastruct. Res.* 73:34–43.
58. Shimizu, T., and K. A. Johnson. 1982. Vanadate-induced inhibition of dynein ATPase from *Tetrahymena*. *Biophys. J.* 37:346a (Abstr.).

59. Stein, L. A., P. B. Chock, and E. Eisenberg. 1981. Mechanism of the actomyosin ATPase: effect of actin on the ATP hydrolysis step. *Proc. Natl. Acad. Sci. U. S. A.* 78:1346–1350.
60. Sturgess, J. M., J. Chao, J. Wong, N. Aspin, and J. A. P. Turner. 1979. Cilia with defective radial spokes. A cause of human respiratory disease. *N. Engl. J. Med.* 300:53–56.
61. Sueoka, N., K. S. Chiang, and J. R. Kates. 1967. Deoxyribonucleic acid replication in meiosis of *Chlyamydomonas reinhardi*. I. Isotope transfer experiments with a strain producing eight zoospores. *J. Mol. Biol.* 25:47–66.
62. Summers, K. E., and I. R. Gibbons. 1973. Effects of trypsin digestion on flagellar structures and their relationship to motility. *J. Cell Biol.* 58:618–629.
63. Takahashi, M., and Y. Tonomura. 1978. Binding of 30S dynein with the B-tubules of the outer doublet of axonemes from *Tetrahymena pyriformis* and adenosine triphosphate-induced dissociation of the complex. *J. Biochem.* 84:1339–1355.
64. Tang, W. Y., C. W. Bell, W. S. Sale, and I. R. Gibbons. 1982. Structure of the dynein-1 outer arm in sea urchin sperm flagella. I. Analysis by separation of subunits. *J. Biol. Chem.* 257:508–515.
65. Telzer, B. R., and L. T. Haimo. 1981. Decoration of spindle microtubules with dynein: evidence for uniform polarity. *J. Cell Biol.* 89:373–378.
66. Tilney, L. H., J. Bryan, D. J. Bush, K. Fujiwara, M. S. Mooseker, D. B. Murphy, and D. H. Snyder. 1973. Microtubules: evidence for 13 protofilaments. *J. Cell Biol.* 59:267–275.
67. Warner, F. D. 1976. Cross-bridge mechanisms in ciliary motility: the sliding-bending conversion. In Cell Motility, R. Goldman, T. Pollard, and J. Rosenbaum, editors. Cold Spring Harbor Laboratory, Cold Spring Harbor, NY. 891–914.
68. Warner, F. D. 1978. Cation induced attachment of ciliary dynein cross-bridges. *J. Cell Biol.* 77:R19–R26.
69. Warner, F. D., and D. R. Mitchell. 1978. Structural conformation of ciliary dynein arms and the generation of sliding forces in *Tetrahymena* cilia. *J. Cell Biol.* 76:261–277.
70. Warner, F. D., D. R. Mitchell, and C. R. Perkins. 1977. Structural conformation of the ciliary ATPase dynein. *J. Mol. Biol.* 114:367–384.
71. Warner, F. D., and N. C. Zanetti. 1978. Properties of microtubule sliding disintegration in isolated *Tetrahymena* cilia. *J. Cell Biol.* 86:436–445.
72. Witman, G. B., and N. Minervini. 1982. Dynein arm conformation and mechanochemical transduction in the eukaryotic flagellum. *In* Eukaryotic and Prokaryotic Flagella. W. B. Amos and J. G. Duckett, editors. *Symp. Soc. Exp. Biol.* 35:203–224.
73. Witman, G. B., J. Plummer, and G. Sander. 1978. *Chlamydomonas* flagellar mutants lacking radial spokes and central tubules. Structure, composition, and function of specific axonemal components. *J. Cell Biol.* 76:729–747.
74. Wolosewick, J. J., and K. R. Porter. 1979. Microtrabecular lattice of the cytoplasmic ground substance. *J. Cell Biol.* 82:114–139.
75. Yano, Y., and T. Miki-Noumura. 1981. Two-headed dynein arm. *Biomedical Res.* 2:73–78.
76. Zanetti, N. C., D. R. Mitchell, and F. D. Warner. 1979. Effects of divalent cations on dynein crossbridging and ciliary microtubule sliding. *J. Cell Biol.* 80:573–588.